

# 1                    **The Transcriptome Architecture of Polyomaviruses**

2

3    Jason Nomburg<sup>1,2,3</sup>, Wei Zou<sup>4</sup>, Thomas C. Frost<sup>1,3</sup>, Chandreyee Datta<sup>5,6,7,8</sup>, Shobha  
4    Vasudevan<sup>5,6,7,8</sup>, Gabriel J. Starrett<sup>9</sup>, Michael J. Imperiale<sup>4,10</sup>, Matthew Meyerson<sup>1,2,11\*</sup>,  
5    James A. DeCaprio<sup>1,3,12\*</sup>

6

7    <sup>1</sup>Department of Medical Oncology, Dana-Farber Cancer Institute, Boston MA

8    <sup>2</sup>Broad Institute of MIT and Harvard, Cambridge, MA

9    <sup>3</sup>Harvard Program in Virology, Harvard University Graduate School of Arts and Sciences,  
10    Boston, MA

11    <sup>4</sup>Department of Microbiology and Immunology, University of Michigan, Ann Arbor,  
12    Michigan

13    <sup>5</sup>Massachusetts General Hospital Cancer Center, Harvard Medical School, 185  
14    Cambridge St, CPZN4202, Boston, MA

15    <sup>6</sup>Department of Medicine, Massachusetts General Hospital and Harvard Medical School,  
16    Boston, MA

17    <sup>7</sup>Center for Regenerative Medicine, Massachusetts General Hospital, Harvard Medical  
18    School, Boston, MA

19    <sup>8</sup>Harvard Stem Cell Institute, Harvard University, Cambridge, MA

20    <sup>9</sup>Laboratory of Cellular Oncology, CCR, NCI, NIH, Bethesda, MD, USA

21 <sup>10</sup>Rogel Cancer Center, Ann Arbor, MI

22 <sup>11</sup>Department of Genetics, Harvard Medical School, Boston, MA

23 <sup>12</sup>Department of Medicine, Brigham and Women's Hospital, Harvard Medical School,  
24 Boston, MA

25

26 \*Correspondence to:

27 James A. DeCaprio

28 james\_decaprio@dfci.harvard.edu

29

30 Matthew Meyerson

31 matthew\_meyerson@dfci.harvard.edu

32

## 33 Abstract

34 Polyomaviruses (PyV) are ubiquitous pathogens that can cause devastating human  
35 diseases. Due to the small size of their genomes, PyV utilize complex patterns of RNA  
36 splicing to maximize their coding capacity. Despite the importance of PyV to human  
37 disease, their transcriptome architecture is poorly characterized. Here, we compare  
38 short- and long-read RNA sequencing data from eight human and non-human PyV. We  
39 provide a detailed transcriptome atlas for BK polyomavirus (BKPyV), an important  
40 human pathogen, and the prototype PyV, simian virus 40 (SV40). We identify pervasive  
41 wraparound transcription in PyV, wherein transcription runs through the polyA site and  
42 circles the genome multiple times. Comparative analyses identify novel, conserved  
43 transcripts that increase PyV coding capacity. One of these conserved transcripts  
44 encodes superT, a T antigen containing two RB-binding LxCxE motifs. We find that  
45 superT-encoding transcripts are abundant in PyV-associated human cancers. Together,  
46 we show that comparative transcriptomic approaches can greatly expand known  
47 transcript and coding capacity in one of the simplest and most well-studied viral families.

48

## 49 Introduction

50 Polyomaviruses (PyV) are ubiquitous pathogens that can cause devastating human  
51 diseases (Jiang et al., 2009a) including polyomavirus-associated nephropathy (PVAN),  
52 hemorrhagic cystitis, and bladder cancer associated with BKPyV (Starrett et al., 2021),  
53 progressive multifocal leukoencephalopathy caused by JCPyV, Merkel cell carcinoma  
54 caused by Merkel cell polyomavirus (MCPyV), and dermatosis caused by human

55 polyomavirus 7 (HPyV7) (Jiang et al., 2009a; Nguyen et al., 2017). PyV have circular  
56 double-stranded DNA genomes and express viral genes with distinct “early” and “late”  
57 kinetics. Early and late transcripts are driven by a bi-directional central promoter, and  
58 each terminate at their own polyA signal sequence located between the early and late  
59 regions. The PyV early region encodes tumor or T antigens that promote cell cycle  
60 progression and facilitate replication of the viral genome by host DNA polymerase. The  
61 PyV late region originating from the common PyV promoter element on the opposite  
62 genome strand encodes the structural proteins required for the generation of progeny  
63 virions.

64

65 PyV transcripts undergo complex splicing to increase their coding capacity in the face of  
66 their small ~5kb genomes. In addition to the major large T (LT) and small T (ST)  
67 antigens, additional T antigen splice forms have been identified including transcripts that  
68 generate truncated versions of LT (17kT, 57kT, truncT, and T' in SV40, MCPyV,  
69 BKPyV, and JCPyV respectively), a “superT” antigen that contains a duplicated LxCxE  
70 RB-binding motif in SV40, middle T (MT) in murine PyV (MPyV), and ALTO in MCPyV  
71 (Abend et al., 2009; Carter et al., 2013; Freund et al., 1992; Kress et al., 1979; Shuda et  
72 al., 2008; Smith et al., 1979; Trowbridge and Frisque, 1995; Zerrahn et al., 1993).

73 Although the diversity of late transcripts has been explored in SV40 (Good et al., 1988),  
74 late transcript diversity in other PyV, including the major human pathogens, is poorly  
75 characterized. To address this lack of knowledge of PyV transcription and to discover  
76 unannotated biologically relevant PyV-encoded protein products, we used long- and



77 short-read RNA sequencing technologies to characterize the transcriptomes of eight  
78 human and non-human PyVs.

79

## 80 Results

### 81 **RNA sequencing expands PyV transcript diversity.**

82 To expand known PyV transcript diversity, we conducted a series of viral infections  
83 followed by total or polyA short-read Illumina RNA sequencing (short-RNAseq (total)  
84 and short-RNAseq (polyA) respectively) (**Figure 1A**). We integrated this newly  
85 generated data with publicly available data from infected cell culture, human skin, and  
86 other settings (**Table 1**). Viruses studied include SV40, BKPyV Dunlop variant and Dik  
87 (wild type, or archetype), JCPyV, MPyV, MCPyV, HPyV7, and bark scorpion  
88 polyomavirus 1 (BSPyV1).

89

90 For SV40 and the BKPyV Dunlop variant, which replicate robustly in cell culture, we  
91 complemented short-read sequencing with Nanopore direct RNA sequencing  
92 (dRNAseq) and PacBio Single-Molecule Real-Time sequencing (SMRTseq) (**Figure**  
93 **1A**), two long-read sequencing approaches for polyA RNA with distinct library  
94 preparations and sequencing strategies. Resultant RNAseq reads from long- and short-  
95 read sequencing strategies were mapped against the viral reference genome and  
96 grouped into transcript classes based on the presence of shared introns as detailed in  
97 the Methods (**Figure 1B**). For SV40, viral transcripts represented 11.6% and 8.8% of

98 transcripts in dRNAseq and SMRTseq, respectively. For BKPyV Dunlop, viral transcripts  
99 represented 28.6% and 27.8% of transcripts in dRNAseq and SMRTseq, respectively.  
100 The total number of viral reads is detailed in **Figure S1A**. Transcripts within the same  
101 class contain the same introns but may have distinct transcript start sites (TSSs) and  
102 transcript end sites (TESs). For most transcriptomes, the majority of transcripts are  
103 members of the first few transcript classes (**Figure S1B**). To filter out erroneous splice  
104 sites, we required that all introns present in a dRNAseq or SMRTseq read must also be  
105 supported by at least 5 splice junction-spanning reads in short-RNAseq (total) data.  
106 Detailed information on this transcript class strategy is present in the Methods.

107

108 Comparison of read coverage from short-RNAseq (total), dRNAseq, and SMRTseq  
109 revealed that dRNAseq and SMRTseq were relatively consistent with read coverage,  
110 generally reflected expected patterns of exon usage (**Figure 1C**). In contrast, the read  
111 coverage of short-RNAseq (total) was less representative of expected viral exon usage  
112 and may reflect noise due to the amplification of smaller RNA fragments (**Figure 1C**).

113

114 For SV40 and BKPyV Dunlop, a transcript class (consisting of transcripts with shared  
115 introns) was considered a bona-fide viral transcript if it was at least 0.1% of late or early  
116 transcripts in dRNAseq or SMRTseq data as described in the Methods. For SV40,  
117 which has detailed splice annotations (Good et al., 1988), we found that dRNAseq and  
118 SMRTseq data are largely consistent with existing annotations. However, we identified  
119 five previously unannotated SV40 transcripts that were supported by both long-read

120 sequencing approaches, plus one additional previously unannotated SV40 transcript  
121 class supported by SMRTseq and short-RNAseq (total) (**Figure 1D, Figure 2**).

122

123 In contrast to SV40 and despite its clinical importance, BKPyV transcripts have been  
124 poorly characterized. We identified a total of 23 transcripts, 21 of which are supported  
125 by both dRNAseq and SMRTseq data and only six of which were previously identified  
126 (Abend et al., 2009; Seif et al., 1979) (**Figure 1E, Figure 3**). While novel BKPyV late  
127 transcripts are often analogous to the characterized wraparound and non-wraparound  
128 transcripts previously identified in SV40, several additional and unexpected BKPyV  
129 early transcripts were identified. For example, an atypically early TSS revealed a splice  
130 donor that was used to generate transcript E3 (**Figure S4**). Early transcripts including  
131 E6, E9, and E11 are conserved across numerous PyV and lead to formation of novel  
132 ORFs - these are described in detail below.

133

134 We generated a comprehensive atlas of SV40 and BKPyV transcripts in **Figures S3 -**  
135 **S8**. Watch plots display the structure of each identified transcript, and read pileups  
136 show all transcripts identified in each transcript class. The relative abundance of each  
137 transcript as well as exact splice coordinates and abundance information for each  
138 identified transcript is provided in **Supplementary Tables 1 and 2**. Transcripts can also  
139 be explored using an interactive Google Colab notebook  
140 ([https://colab.research.google.com/github/jnoms/SV40\\_transcriptome/blob/main/bin/colab/PyV\\_exploratory.ipynb](https://colab.research.google.com/github/jnoms/SV40_transcriptome/blob/main/bin/colab/PyV_exploratory.ipynb)). A comprehensive analysis of all splice sites detected in short-

142 read short-RNAseq (total) and short-RNAseq (polyA) in eight PyV studied is presented  
143 in **Figure S9**.

144

145 To address the possibility that distinct transcript isoforms could be preferentially  
146 translated, we performed polysome profiling of SV40-infected cells coupled with  
147 dRNAseq of whole-cell and polysome-associated polyadenylated RNAs (**Figure 1F**).  
148 The ribosome occupancy, determined as the ratio between a transcript's normalized  
149 polysome abundance and its normalized whole-cell abundance, has a mean of slightly  
150 above 1 for host transcripts (**Figure S2D**). We found 11.2% of reads in the whole-cell  
151 fraction and 18.7% in the polysome fraction were viral, consistent with active translation  
152 of viral transcripts. For late transcripts, the relative abundance in the whole-cell fraction  
153 was tightly coupled to polysome relative abundance (**Figure 1G**), indicating limited  
154 preferential translation of late transcripts. In contrast to late transcripts, we found that  
155 the LT:ST ratio was 1.3:1 in the polysome fraction compared to a 3.4:1 ratio of LT:ST  
156 transcripts in the whole-cell fraction, indicating preferential translation of ST during  
157 infection.

158

### 159 **Wraparound transcription is conserved across diverse PyV.**

160 Long-read sequencing revealed the existence of many late transcripts that contain  
161 multiple copies of a duplicated leader exon. Leader-leader splicing is due to  
162 “wraparound transcription” of PyV transcripts that failed to terminate at the late  
163 polyadenylation signal and continue to circle the genome repeatedly. PyV wraparound

164 transcription has been described previously although the structure and diversity of these  
165 RNA species is unknown (Adami et al., 1989; Garren et al., 2015; Luo and Carmichael,  
166 1991; Reddy et al., 1978). We investigated these transcripts in dRNAseq data from  
167 SV40 and BKPyV. To supplement these data, we also performed dRNAseq on MPyV-  
168 infected cells. Wraparound transcription, defined by the presence of repetitive copies of  
169 a shared leader sequence, was found in long-read sequencing for all three PyVs  
170 (**Figure 4A, B, C**: note the presence of the leader-leader or repeated exon near the “11  
171 o’clock” position in watch plots). In addition to this leader sequence repetition, there are  
172 diverse forms of wraparound transcripts that contain various combinations of  
173 subsequent introns and encode for distinct viral proteins (**Figure 2, 3**). While only 3.6%  
174 of SV40 transcripts originate from wraparound transcription, BKPyV and MPyV have  
175 markedly higher rates at 25% and 41% respectively (**Figure 4D**).

176

177 Next, we inferred the presence of wraparound transcription in diverse PyV by identifying  
178 short-RNAseq (total) reads that span the leader-leader junction (**Figure 4E**). Despite the  
179 limited length of these short reads, leader-leader junctions can be accurately identified  
180 within a single read through analysis of junction sites (**Figure 4F**). We found evidence of  
181 wraparound transcription in all eight PyV investigated here. This includes HPyV7  
182 RNAseq from infected human skin and RNAseq data from a scorpion containing the  
183 highly divergent Bark scorpion polyomavirus 1 (BSPyV1), indicating that wraparound  
184 transcription occurs *in vivo* and is widely conserved across PyV.

185

186 **Pervasive premature polyadenylation of early transcripts in SV40, BKPyV, and**  
187 **MPyV.**

188 We found that many early transcripts in SV40 and BKPyV underwent alternative  
189 polyadenylation (APA) earlier than the canonical polyA site as indicated by premature  
190 transcript end positions near 3 o'clock in the watch plots (**Figure S10A, B**). Early  
191 transcript APA had been previously identified in MPyV, where there is a canonical polyA  
192 signal sequence (AATAAA) within the LT ORF (Kamen et al., 1980b; Norbury and Fried,  
193 1987). Indeed, dRNAseq identified APA of early transcripts in MPyV-infected cells  
194 (**Figure S10C, D**). In contrast to MPyV, APA in SV40 and BKPyV may be driven by  
195 alternative polyA signal sequences to the 5' of the APA site (ATTAAA in SV40,  
196 AAGAAA or TATAAA in BKPyV). Assessment of the cumulative incidence of early  
197 transcript termination shows abrupt increases in transcript termination ~1500nt  
198 upstream of the canonical polyA site in all three viruses (**Figure S10D**). This APA  
199 appears to be similarly abundant in LT and ST transcripts. We found that transcripts  
200 with APA still contain a full polyA tail that, while shorter than the polyA tails of transcripts  
201 that use the canonical polyA site, still tend to be longer than the polyA tails of host  
202 transcripts (**Figure S10E, S10F, S10G, S2C**). The polyA tail length of a spike-in control  
203 RNA with a known 30-adenine polyA tail was correctly estimated by dRNAseq (**Figure**  
204 **S2C**). We find that transcripts containing APA can associate with polysomes (**Figure**  
205 **S10H, I**), indicating that these transcripts are translated.

206

207 **Comparative analysis of short-RNAseq (total) data reveals conserved,**  
208 **unannotated splice-forms that may generate variant ORFs.**

209 Next, we conducted a comparative analysis of PyV transcription from short-RNAseq  
210 (total) data (**Figure S9**), with the hypothesis that data from diverse PyV could reveal  
211 unannotated splice forms. This analysis led to the discovery of several unannotated but  
212 conserved splicing events that have the potential to expand the coding capacity of PyV  
213 (**Figure 5**).

214

215 We found that PyVs including HPyV7, MPyV, BKPyV Dunlop, and MCPyV express a  
216 transcript utilizing the LT first exon donor but an acceptor within the ST ORF leading to  
217 the generation of the ST2 ORF (**Figure 5A**). This splice occurs in-frame in HPyV7 and  
218 BKPyV resulting in an internal deletion within ST, while in MPyV and MCPyV this splice  
219 lands out of frame and results in the addition of novel C-terminal amino acids. The ST2  
220 splice is highly abundant in HPyV7 representing over 20% of spliced early transcripts  
221 from HPyV7-infected human skin. ST2-encoding transcripts were detected in BKPyV  
222 dRNAseq and SMRTseq data (transcript E6).

223

224 MPyV encodes MT in addition to the LT and ST antigens common with other PyV.  
225 MPyV MT is generated from a splicing event that connects the ST ORF with an ORF in  
226 the alternative frame of the LT second exon. To our surprise, we found that BKPyV  
227 expresses low levels of a similar transcript containing a splice that connects the ST  
228 ORF with an MT-like ORF likewise in an alternative frame of the LT second exon  
229 (**Figure 5B**). This MT transcript was also detected in BKPyV dRNAseq and SMRTseq  
230 data (transcript E9).

231

232 JCPyV encodes two VP1 variants, VP1Xs, that consist of the N-terminal region of VP1  
233 with novel C-termini that make up as much as 30% of late spliced transcripts in JCPyV  
234 (**Figure 5C**) and have been recently identified and validated by an independent group  
235 (Saribas et al., 2018). We found that VP1X-encoding transcripts were also produced by  
236 MCPyV, SV40, BKPyV, and MPyV, albeit at a lower abundance than in JCPyV. Except  
237 for one JCPyV VP1X-encoding splice, these transcripts were generated from splicing of  
238 wraparound transcripts that run through the late polyA signal sequence.

239

240 **SuperT, a T antigen containing two RB-binding motifs, is present in multiple PyV**  
241 **and in PyV-associated human cancers.**

242 Studies in SV40-transformed cells previously identified a superT antigen with higher  
243 molecular weight than LT, containing a duplicated region with two copies of the LxCxE  
244 RB-binding motif (Eul and Patzel, 2013). We found that a superT-specific splice was  
245 present in SV40, BKPyV (Dik and Dunlop variants), JCPyV, and MCPyV during viral  
246 infection (**Figure 5D**). The superT-specific splice originates from a splice donor  
247 canonically associated with a conserved truncated LT antigen (17kT in SV40, truncT in  
248 BKPyV, 57kT in MCPyV, and T' in JCPyV), but uses the LT second exon acceptor  
249 available due to wraparound transcription. We find evidence of superT in the dRNAseq  
250 and SMRTseq data for SV40 and BKPyV Dunlop infections (transcripts E4 and E11  
251 respectively). Western blot with an antibody reactive to LT in BKPyV Dik-infected cells  
252 revealed a band with slightly higher molecular weight than LT that is consistent with



253 superT (**Figure 5F**). BKPyV Dik mutant M1, designed to remove ST by replacing the LT  
254 intron with an intron from the plasmid pCI (**Figure 5E**), also generated a superT band of  
255 expected size. BKPyV Dik mutant M2 was generated by removing the LT intron and  
256 adding the pCI intron just 5' of the LT first exon. Should the truncT donor be used to  
257 generate superT in this mutant, the only available acceptor is before the LT 1<sup>st</sup> exon,  
258 which would result in the formation of an aberrantly larger superT due to the inclusion of  
259 a second copy of the LT first exon (**Figure 5E**). short-RNAseq (polyA) analysis of cells  
260 infected with BKPyV Dik WT, M1, or M2 show junctions consistent with this model  
261 (**Figure S11**), and western blot revealed that the superT band in M2 is shifted to a  
262 higher molecular weight (**Figure 5F**). Together, these data indicate that superT is  
263 generated by BKPyV Dik during viral infection.

264

265 SuperT was initially identified as an unexplained higher-molecular weight T antigen  
266 present in many SV40-transformed cell lines (Kress et al., 1979; Smith et al., 1979).  
267 While superT can be generated during viral infection because of wraparound  
268 transcription, in SV40-transformed cells it would be possible to yield pre-mRNAs that  
269 can be spliced to form superT should the virus be integrated in tandem copies (**Figure**  
270 **6A**). Indeed, we previously observed that MCPyV integration events in Merkel cell  
271 carcinoma (MCC) often lead to partial duplications of the viral genome and result in the  
272 tandem insertion of multiple copies of viral early genes (Starrett et al., 2020).  
273 Furthermore, the duplicated region in superT includes the RB-binding LxCxE motif,  
274 raising the possibility that superT can function as a potent oncogene. We therefore  
275 asked if there is evidence of superT in PyV-associated human cancers.

276

277 To address this question, we first analyzed short-RNAseq (total) data from five BKPyV-  
278 associated bladder cancers (Starrett et al., 2021). To our surprise, we found that short-  
279 RNAseq (total) data from two replicates of one BKPyV-associated bladder cancer  
280 contained a higher abundance of superT-specific splice than even the LT- or ST-specific  
281 splices, suggesting that a large fraction of “LT” in this tumor is superT (**Figure 6B**). We  
282 next analyzed short-RNAseq (polyA) data from a series of 30 MCPyV-positive MCCs  
283 and found evidence of superT in six cases (**Figure 6B**). Notably, the total number of  
284 viral reads in some MCPyV-positive but superT-null tumors was very low, leaving open  
285 the possibility that sequencing depth was insufficient to identify the superT splice in  
286 additional tumors. Using PCR and sanger sequencing, we confirmed the presence of  
287 the superT splice in MCC tumor J45\_440 (**Figure S12A**).

288

289 We hypothesized that superT may be generated by cis-splicing due to concatemeric  
290 integration of multiple copies of the etiologic PyV in these tumors (**Figure 6A**). To  
291 address this hypothesis, we investigated three MCCs (J45\_440, J17\_296, J11\_285) for  
292 which we possess short-read whole genome sequencing data. From J11\_285, we were  
293 able to assemble the entire integration site, showing that MCPyV is integrated in a  
294 manner that could allow cis-splicing to generate superT (**Figure S12B**). For J45\_440,  
295 we assembled a single viral block integrated in chromosome 7 (**Figure S12C**). We  
296 found that 1) there are likely 2 copies of the viral genome, and 2) the 5' viral integration  
297 site appears to fall on chromosome 7 “after” the 3' viral integration site, observations  
298 consistent with the existence of two copies of the viral genome in tandem separated by

299 a small segment of host DNA at this integration site. For J17\_296, from the assembly,  
300 we could infer three distinct segments of viral DNA with integration sites closely spaced  
301 within chromosome 2 (**Figure S12D**), indicating a complex integration pattern. The  
302 longer block contains two copies of the early region and can likely support superT  
303 generation through cis-splicing. The LT ORF of MCPyV is often truncated by premature  
304 stop codons or deletions in MCC. We found that a stop codon in J17\_296 likely  
305 prevents expression of superT, but no stop codons occur before the superT splice in  
306 J45\_440 or J11\_285 (**Figure S12E**). Together, these data indicate that viral integration  
307 sites often could support cis-splicing to generate superT.

308 Two recent studies have found evidence of circular RNAs (circRNAs) that may be  
309 generated by MCPyV in MCC and may support the translation of ALTO (Abere et al.,  
310 2020; Yang et al., 2021). Of note, the major circRNA splice is equivalent to our  
311 proposed MCPyV superT splice - a short-RNAseq read spanning the proposed circRNA  
312 junction cannot be differentiated from a read spanning the superT junction. However,  
313 the MCC RNAseq samples in which we found superT are short-RNAseq (polyA), which  
314 should select against the potential circRNA due to its lack of a polyA tail. Furthermore,  
315 we detect the superT splice in short-RNAseq (polyA) of SV40 and BKPyV Dunlop  
316 infections in cell culture (**Figure S9**), although at around ~2/3 of its relative abundance  
317 in short-RNAseq (total). Finally, we identify full-length superT transcripts in dRNAseq  
318 data, which is highly unlikely to sequence circRNA since it is not polyadenylated. This  
319 leaves open the possibility that some superT-like splice in short-RNAseq (total) from  
320 viral infection originates from circRNA but suggests that most are from linear transcripts  
321 that contain a polyA tail.

322

## 323 Discussion

324 Here, we show that leveraging multiple long- and short-read RNA sequencing  
325 approaches across 8 polyomaviruses has allowed us to greatly expand known transcript  
326 diversity of this viral family. Short read RNAseq has limited capacity to characterize  
327 transcriptome diversity because only a small fraction of reads span splice junctions, and  
328 these junctions often cannot be phased with other junctions or to the transcript start and  
329 end sites. Integrating long-read sequencing has allowed sequencing of entire  
330 transcripts, including phasing of splice sites and transcript start and end positions.  
331 Recent studies have leveraged long read sequencing to shed light on exceptional  
332 complexity in the transcriptomes of diverse RNA and DNA viruses (Balázs et al., 2017;  
333 Depledge et al., 2019; Garalde et al., 2018; Keller et al., 2018; Kim et al., 2020;  
334 Nomburg et al., 2020; Price et al., 2020). We have expanded these studies to show that  
335 a comparative approach within a viral family can identify conserved transcripts that  
336 extend viral coding capacity.

337

338 Historically, studies of PyV transcripts were limited by the sensitivity and resolution of  
339 northern blots, or by the read length of short read sequencing. Despite these limitations,  
340 studies in the 70's and 80's were able to cumulatively characterize several SV40 late  
341 transcripts, including one containing leader-leader splicing (Ghosh et al., 1978; Good et  
342 al., 1988; Reddy et al., 1978). In contrast to SV40, the architecture of BKPyV late  
343 transcripts is poorly characterized - prior to this work, the two major classes of late

344 transcripts (“16S” and “19S”, reflecting transcript size based on gradient sedimentation  
345 properties) were the primary late transcript classifications (Seif et al., 1979). Only  
346 recently did a study provide some evidence for leader-leader splicing in BKPyV (Zou et  
347 al., 2020). While the late transcripts of most PyV are thought to encode the canonical  
348 late viral proteins, a recent study in JCPyV identified two splice events that lead to the  
349 generation of novel proteins containing the N-terminal region of VP1 - one of which was  
350 validated through western blot (Saribas et al., 2018). We found that these transcripts  
351 (deemed “VP1X”) are highly expressed in JCPyV but are also expressed at lower level  
352 in BKPyV, MPyV, MCPyV, and SV40.

353

354 Leader-leader splicing is known to be highly prevalent in MPyV, where as many as 12  
355 leader exons have been observed on a single RNA (Kamen et al., 1980a; Legon et al.,  
356 1979; Treisman, 1980) - in our data, we have identified over 15 leader exons in a single  
357 transcript. Furthermore, leader-leader splicing is required for stable accumulation of  
358 MPyV late transcripts, dependent on length but not nucleotide composition of the leader  
359 (Adami et al., 1989). Despite these observations, the exact structure, diversity, and  
360 conservation of wraparound transcripts was not understood. Here, we found that leader-  
361 leader splicing and wraparound transcription occurs in all PyV studied, including in the  
362 divergent Bark scorpion polyomavirus 1, and found that the prevalence of leader-leader  
363 splicing varies significantly between PyV. It is possible that this variation reflects  
364 differences in the strength of the late polyA signals of these PyV. We found a large  
365 diversity of wraparound transcripts containing variable numbers of the leader sequence  
366 and diverse patterns of subsequent exon usage.

367

368 While late and early transcripts are thought to primarily end at the canonical late or early  
369 polyadenylation sites, studies previously observed APA of early transcripts in MPyV  
370 (Kamen et al., 1980b; Norbury and Fried, 1987). Here, we likewise identify pervasive  
371 APA of early SV40 and BKPyV Dunlop transcripts and find that SV40 early transcripts  
372 with APA can associate with polysomes and are likely translated. In addition, polysome  
373 profiling revealed that SV40 transcripts are higher abundance in polysome-associated  
374 RNAs than in whole-cell RNA populations, indicating preferential translation of SV40  
375 transcripts. The relative abundance of individual late viral transcripts in the polysome  
376 closely reflected their whole-cell abundance - conversely, ST transcripts were  
377 preferentially translated compared to LT transcripts. The mechanism driving this  
378 difference needs further study, as these transcripts differ only by a minor difference in  
379 splice donor usage.

380

381 In addition to the major early transcripts encoding LT and ST, other early transcripts  
382 have been identified in some PyV. MPyV encodes MT, generated by a splice  
383 connecting the ST ORF and an ORF overprinted with LT second exon. MT is a primary  
384 oncogene in MPyV and was thought to be largely restricted to rodent PyVs (Gottlieb and  
385 Villarreal, 2001). We found that BKPyV generates a MT-like ORF through splicing  
386 connecting ST and an ORF similarly overprinted with the LT second exon, showing that  
387 non-rodent PyVs may be capable of expressing MT-like ORFs. In addition, MPyV also  
388 encodes a tinyT antigen consisting largely of the LT first exon, resulting from a splice  
389 connecting the LT first exon donor and MT acceptor (Riley et al., 1997). We identified a

390 novel T antigen, ST2, that is generated from a splice from the LT first exon donor to a  
391 splice acceptor within the ST ORF. This transcript is highly expressed in HPyV7 and  
392 present at lower levels in BKPyV, MPyV, and MCPyV. Many PyV encode a truncated  
393 variant of LT - this includes SV40 17kT, BKPyV truncT, MCPyV 57kT and JCPyV T'  
394 proteins (Abend et al., 2009; Shuda et al., 2008; Trowbridge and Frisque, 1995; Zerrahn  
395 et al., 1993). These transcripts contain a canonical LT splice and a subsequent splice  
396 that removes a large portion of the LT ORF.

397

398 We found that the same secondary splice sites responsible for truncated LT variants  
399 can be used to generate superT. superT was initially observed in many SV40-  
400 transformed cell lines (Kress et al., 1979; Smith et al., 1979) - in a similar manner, we  
401 find that concatemeric integration of BKPyV and MCPyV in human cancers can facilitate  
402 the generation of superT. We also find that superT is generated in lytic infections of  
403 SV40, BKPyV, MCPyV and JCPyV. Eul and colleagues have published several studies  
404 proposing that SV40 superT can be generated by trans-splicing between two separate  
405 pre-mRNAs in the context of artificial expression constructs encoding the SV40 early  
406 region (20, 31, 32). However, we find that in MCC tumors that generate superT and for  
407 which we can assemble the viral integration site, the viral genome is likely integrated in  
408 tandem in a way that could facilitate the cis-splicing of pre-mRNA that spans multiple  
409 genome copies. Thus, while we cannot rule out trans-splicing from these data, we  
410 believe cis-splicing is more likely. Future studies are necessary to understand the  
411 biology of superT including its oncogenic potential and ability to bind multiple RB  
412 molecules. Finally, efforts should be taken to understand if superT is expressed by PyV

413 and contributes to disease in other contexts, such as by BKPyV in PVAN or JCPyV in  
414 PML.

415

416 We show that complex, uncharacterized splicing events are used by PyV to expand  
417 their protein coding capacity. Future work is necessary to understand the biological  
418 function of these transcripts and proteins. It is possible that unannotated splicing we  
419 identify here could be differentially abundant in other biological contexts, so it will be  
420 important to investigate PyV splicing in other infection contexts and human diseases.  
421 Future transcriptome analyses that integrate long and short reads from multiple viruses  
422 may have utility to expand characterized transcript and coding capacity in other viral  
423 families.

424

## 425 Conclusions

426 We provide a comprehensive transcriptome atlas for the prototype PyV SV40, as well  
427 as the critically important human pathogen BKPyV. Comparative analyses of PyV  
428 transcriptomes reveals conserved splice events that may expand PyV coding capacity.  
429 We find that superT, a transcript generated by SV40, BKPyV, JCPyV, and MCPyV that  
430 encodes a T antigen containing two RB-binding LxCxE domains, is present in several  
431 PyV-associated human cancers. Together, these data expand our understanding of PyV  
432 transcriptomes and uncover unannotated PyV-encoded proteins of potential relevance  
433 to human disease.



434

435

## 436 Materials and Methods

### 437 **Data and code availability.**

438 All code used in this project can be found at the zenodo and github links below. The  
439 zenodo repository also contains all processed data necessary to reproduce all analyses  
440 and figures. The main processing steps used to process RNAseq data are present as  
441 nextflow pipelines which call modular bash and python scripts.

442 Zenodo: <https://doi.org/10.5281/zenodo.5593468>

443 Github: [https://github.com/jnoms/SV40\\_transcriptome](https://github.com/jnoms/SV40_transcriptome)

444

445 Furthermore, a series of interactive Google Colab notebooks can download all  
446 processed data from Zenodo and completely reproduce all analyses and non-schematic  
447 primary figures. The colab documents are stored on github at

448 [https://github.com/jnoms/SV40\\_transcriptome/tree/main/bin/colab](https://github.com/jnoms/SV40_transcriptome/tree/main/bin/colab). Direct links to the

449 Google Colab documents are as follows:

450 Figure 1:

451 [https://colab.research.google.com/github/jnoms/SV40\\_transcriptome/blob/main/bin/cola](https://colab.research.google.com/github/jnoms/SV40_transcriptome/blob/main/bin/cola)

452 [b/Figure1.ipynb](#)

453 Figure 4:

454 [https://colab.research.google.com/github/jnoms/SV40\\_transcriptome/blob/main/bin/cola](https://colab.research.google.com/github/jnoms/SV40_transcriptome/blob/main/bin/cola)

455 [b/Figure4.ipynb](#)

456 Figure 6:

457 [https://colab.research.google.com/github/jnoms/SV40\\_transcriptome/blob/main/bin/cola](https://colab.research.google.com/github/jnoms/SV40_transcriptome/blob/main/bin/cola)

458 [b/Figure6.ipynb](#)

459

460 A Google Colab notebook is available for interactive investigation of all SV40 and

461 BKPyV viral transcript classes, and does not require computational skills to use:

462 [https://colab.research.google.com/github/jnoms/SV40\\_transcriptome/blob/main/bin/cola](https://colab.research.google.com/github/jnoms/SV40_transcriptome/blob/main/bin/cola)

463 [b/PyV\\_exploratory.ipynb](#)

464

465 All raw RNA sequencing data are available at the NCBI sequence read archive at

466 accession **XXXXXX**.

467

## 468 **Datasets**

469 Information on all samples and viruses (excluding tumors) can be found in **Table 1**.

Table 1				
Virus	Sequencing Type	Origin (Accession)	MOI / Timepoint	Host

SV40	dRNAseq (two replicates)	Generated here	MOI 1 / 48hpi	<i>C. Sabaeus</i>
SV40	SMRTseq	Generated here	MOI 1 / 48hpi	<i>C. Sabaeus</i>
SV40 (polysome input/whole-cell)	dRNAseq	Generated here	MOI 1 / 44hpi	<i>C. Sabaeus</i>
SV40 (polysome)	dRNAseq	Generated here	MOI 1 / 44hpi	<i>C. Sabaeus</i>
SV40	Short-RNAseq (total)	Generated here	MOI 1 / 48hpi	<i>C. Sabaeus</i>
SV40	short-RNAseq (polyA)	Generated here	MOI 1 / 48hpi	<i>C. Sabaeus</i>
BKPyV (Dunlop)	dRNAseq	Generated here	MOI 0.5 / 3dpi	Human
BKPyV (Dunlop)	SMRTseq	Generated here	MOI 0.5 / 3dpi	Human
BKPyV (Dunlop)	Short-RNAseq (total)	Generated here	MOI 0.5 / 3dpi	Human
BKPyV (Dunlop)	short-RNAseq (polyA)	Generated here	MOI 0.5 / 3dpi	Human
BKPyV (Dik) WT	Short-RNAseq (total)	Generated here	MOI 1 / 5dpi	Human
BKPyV (Dik) WT	Short-RNAseq (polyA)	Generated here	MOI 1 / 5dpi	Human
BKPyV (Dik) M1	Short-RNAseq (polyA)	Generated here	MOI 1 / 5dpi	Human

BKPyV (Dik) M2	Short-RNAseq (polyA)	Generated here	MOI 1 / 5dpi	Human
MPyV	dRNAseq	Generated here	Unknown / 28hpi	Mouse
MPyV	Short-RNAseq (total)	Garren et al. (Garren et al., 2015) (SRR2043214)	MOI 50 / 36hpi	Mouse
JCPyV	Short-RNAseq (total)	Assetta et al. (Assetta et al., 2016) (SRR9967610)	Unknown / 9dpi	Human
MCPyV (Synthetic genome)	short-RNAseq (polyA)	Theiss et al. (Theiss et al., 2015) (EBI: ERS760222)	200ng viral DNA / Unknown	Human
HPyV7	Short-RNAseq (total)	Rosenstein et al. (Rosenstein et al., 2021) (SRR11488976, SRR11488977)	From infected human skin	Human
BSPyV1	Short-RNAseq (total)	Identified by Schmidlin et al. (Schmidlin et al., 2021) (SRR5958578)	From whole scorpion	C. <i>sculpturatus</i>

470

#### 471 **Tumor samples**

472 The BKPyV-associated bladder cancer is sample TBC03 that has been described  
473 (Starrett et al., 2021). This sample is stranded, short-RNAseq (total).

474

475 Merkel cell carcinoma samples: Sections of tissue were isolated from patient-derived  
476 tumor biopsies and suspended in RNAlater (Thermo Fischer) until further processing.

477 RNA and DNA was extracted from each section via the AllPrep DNA/RNA kit (Qiagen).  
478 Isolated RNA and DNA were each sequenced (PE150) on the NovaSeq 6000 platform  
479 (Illumina) for a depth of 50 M reads or 60x genomic coverage per sample, respectively  
480 (Novogene). RNAseq data are unstranded, short-RNAseq (polyA).

481

#### 482 **SV40 infection and RNA extraction**

483 BSC40 cells (ATCC CRL-2761) were seeded on 150mm dishes at  $5.37 \times 10^6$  cells per  
484 plate - about 70% confluence. After waiting 4 hours for the cells to adhere, cells were  
485 infected with SV40 at MOI 1 as previously described (Tremblay et al., 2001) with slight  
486 modification. In brief, maintenance media was removed, and each 150mm dish was  
487 inoculated with 6mL of virus stock diluted in DMEM + 2% FBS. Infection was allowed to  
488 proceed at 37°C, 5% CO<sub>2</sub> for one hour, with the plates rocked every 15 minutes to  
489 ensure adequate coverage of the solution over the cell monolayer. At the end of this  
490 period, DMEM + 2% FBS was added to a final volume of 25mL per 150mm dish. Each  
491 dish was then incubated at 37°C, 5% CO<sub>2</sub> for 48 hours. RNA was extracted using the  
492 QIAGEN RNeasy Mini Plus Kit (QIAGEN 74134). This total RNA was then subjected to  
493 Nanopore direct RNA sequencing and Illumina total- and polyA-RNA sequencing as  
494 described below.

495

#### 496 **BKPyV infection and RNA extraction**

497 Archetype and rearranged BKPyV (Dik and Dunlop, respectively) were purified and  
498 titrated as described (Jiang et al., 2009b). RPTE-hTERT cells (Zhao and Imperiale,

499 2019) were plated in 6-well plate and prechilled for 15 min at 4°C and infected with Dik  
500 or Dunlop at a MOI of 1 and 0.5 fluorescence-forming unit (FFU)/cell, respectively. The  
501 cells were incubated at 4°C for 1 h with gentle shaking every 15 min. The virus was  
502 removed and fresh REGM medium was added to the cells. Dik and Dunlop infected  
503 cells were collected at 120 hpi and 96 hpi, respectively. Total RNA was extracted using  
504 the Direct-zol RNA MiniPrep kit (ZYMO Research, USA). This total RNA was then  
505 subjected to Nanopore direct RNA sequencing and Illumina total- and polyA-RNA  
506 sequencing as described below.

507

#### 508 **MPyV infection and RNA extraction**

509 C57 mouse embryo fibroblasts (ATCC SCRC-1008) were plated on a 150mm dish at  
510 40% confluence. After several hours of growth, the typical DMEM + 10% FBS media  
511 was replaced with serum free DMEM. The next day, the crude viral stock was thawed at  
512 37°C, incubated at 45°C for 20 minutes to facilitate the final liberation of virus into the  
513 supernatant, and cell debris removed from the viral stock with centrifugation. The  
514 prepared virus stock was then diluted 1:10 with an absorption buffer consisting of HBSS  
515 with 10mM HEPES, 1% FBS, at pH 5.6. Media was removed from the target cells, and  
516 6mL of diluted virus in absorption buffer was added. Infection was allowed to proceed at  
517 37°C, 5% CO<sub>2</sub> for one hour, with the plates rocked every 15 minutes to ensure  
518 adequate coverage of the solution over the cell monolayer. At the end of this period, the  
519 absorption buffer was removed and DMEM + 2% FBS was added to a final volume of  
520 25mL per 150mm dish. Cells were inoculated for 28 hours at 37°C, 5% CO<sub>2</sub>, after which  
521 RNA was extracted using TRIzol (ThermoFisher 15596026) according to the

522 manufacturer's instructions. This total RNA was then subjected to Nanopore direct RNA  
523 sequencing as described below.

524

525 The virus stock used here was kindly provided by the lab of Robert Garcea. This virus  
526 stock (viral strain NG59RA) was a crude supernatant from MPyV-infected cells originally  
527 generated by the lab of Thomas Benjamin on 02/08/2011 and was of unknown titer.  
528 This stock was subjected to a total of three freeze-thaw cycles before use.

529

### 530 **SV40 polysome profiling**

531 BSC40 cells were plated on 4 150mm dishes at 60% confluence. After waiting 4 hours  
532 for the cells to adhere, cells were infected with SV40 at MOI 1 as reported above. At 44  
533 hours post infection cell culture media was replaced with media containing 100ug/mL  
534 cycloheximide and incubated for 5 minutes. Plates were placed on ice, media  
535 discarded, and cells were scraped into PBS containing 100ug/mL cycloheximide. Cells  
536 were spun down, the PBS discarded, and cells were lysed in a lysis buffer containing  
537 10mM Tris (pH 8), 100mM KCl, 10mM MgCl<sub>2</sub>, 2mM DTT, 1% Triton X100, 100ug/mL  
538 cycloheximide, and 1unit/uL SUPERase RNase inhibitor (Thermo AM2694). Lysates  
539 were incubated on ice for 20 minutes with intermittent tapping, and then spun at  
540 10,000g for 10 minutes at 4°C. The supernatant was loaded onto a 10-55% sucrose  
541 gradient followed by ultracentrifugation (Beckman Coulter Optima XPN-100  
542 ultracentrifuge) at 32,500 × rpm at 4 °C for 80 minutes in the SW41 rotor. Gradients  
543 were prepared with a gradient mixer and pump. Samples were separated by density

544 gradient fractionation system (Biocomp Piston gradient fractionator IP). RNA was  
545 extracted from reserved input (“whole-cell”) lysate, as well as the polysome fraction  
546 using TRIzol. Equal volumes of each fraction containing heavy polysomes (>2) was  
547 pooled prior to extraction (Lee et al., 2020).

548

### 549 **Western blotting**

550 Infection of wildtype Dik and two Dik mutants in RPTE-hTERT cells was performed as  
551 mentioned above. Protein samples were harvested in E1A buffer with protease and  
552 phosphatase inhibitors, electrophoresed, transferred, and probed with large tumor  
553 antigen antibody (pAb416) as previously described (Zhao and Imperiale, 2019).

### 554 **RNA sequencing**

555 The concentration of total RNA was determined using the Qubit Fluorometer with the  
556 Qubit RNA HS Assay Kit (ThermoFisher Q32852). RNA quality was then assessed on  
557 an Agilent Bioanalyzer and the RNA 6000 Pico Kit (Agilent 5067-1513). PolyA RNA was  
558 isolated using the NEBNext Poly(A) mRNA Magnetic Isolation Module (NEB E7490S)  
559 with an input of 5ug of total RNA - for SV40 and BKPyV Dunlop, up to 8 total reactions  
560 were used to yield sufficient polyA RNA (500ng) for subsequent protocols. In the case of  
561 MPyV, due to limited amounts of total RNA, three reactions were used to yield roughly  
562 100ng of polyA RNA. PolyA RNA concentration was determined again using the Qubit  
563 RNA HS Assay Kit (ThermoFisher Q32852). PolyA RNA was then concentrated to 9uL  
564 using a centriVap.

565



566 500ng of polyA RNA (or, in the case of MPyV, 100ng) in 9uL was then processed using  
567 the Nanopore Direct RNA sequencing kit (SQK-RNA002). Resultant libraries were  
568 sequenced for up to 24 hours on a MinION using an R9.4.1 flow cell.

569

570 In the case of polysome profiling: extracted RNA from the input and polysomes were  
571 separately subjected to 5 reactions each of the NEBNext Poly(A) mRNA Magnetic  
572 Isolation Module using 5ug RNA input per reaction. All resultant polyA RNA was then  
573 processed using the Nanopore Direct RNA sequencing kit (SQK-RNA002). Resultant  
574 libraries were sequenced for up to 24 hours on a MinION-Mk1C using an R9.4.1 flow  
575 cell.

576

577 Illumina total RNA sequencing and polyA RNA sequencing of SV40-, BKPyV Dunlop-,  
578 and BKPyV Dik-infected cells was conducted by Novogene Corporation Inc. The QC for  
579 the RNA samples was performed using Qubit and Bioanalyzer instruments. Libraries  
580 were then prepared using NEBNext Ultra II with RiboZero Plus kit (for short-RNAseq  
581 (total)) and NEBNext Ultra II with PolyA Selection kit (for short-RNAseq (polyA)). Both  
582 library approaches are strand-specific. Library quality and concentration was assessed  
583 with Labchip and qPCR. Libraries were sequenced on NovaSeq6000 using PE150  
584 sequencing.

585

586 PacBio SMRT sequencing of SV40 and BKPyV Dunlop was conducted by the Georgia  
587 Genomics and Bioinformatics Core. Each sample was subjected to IsoSeq library

588 preparation and sequenced on an individual 8M SMRT cell for 26 hours on a Sequel-II  
589 machine.

590

### 591 **Initial Sequence Processing**

592 Raw Nanopore dRNAseq reads from standard SV40, BKPyV Dunlop, and MPyV  
593 infections were basecalled with Guppy version 4.2.2 with the following command:  
594 `guppy_basecaller -i fast5 -s basecalled --flowcell FLO-MIN106 --kit SQK-RNA002 -r --`  
595 `trim_strategy rna --reverse_sequence true --u_substitution true --`  
596 `cpu_threads_per_caller 10`

597

598 Raw Nanopore dRNAseq reads from polysome profiling of SV40 transcripts were  
599 basecalled on a MinION-Mk1C using MinKNOW version 21.02.2.

600

601 PacBio SMRTseq subreads were processed using ccs (version 6.0.0). Full-length,  
602 nonchimeric reads were then generated using the lima (version 2.0.0) and Isoseq3  
603 (version 3.4.0) packages provided by PacBio.

604

605 Stranded Illumina short-RNAseq (total) and short-RNAseq (polyA) reads were  
606 processed in the following way: Files containing read 1 (R1) and read 2 (R2) were  
607 trimmed and adapters removed using Trim Galore! (Krueger, 2016). Next, reads in R1  
608 files were reverse complemented to orient the reads correctly relative to the transcript of

609 origin, and all read headers in the R1 and R2 files were labeled with “\_1” or “\_2”  
610 respectively. The R1 and R2 files were then concatenated. This Illumina processing  
611 pipeline is available in `process_illumina.nf`.

612

613 The MCC tumor RNAseq assessed in this manuscript were short-RNAseq (polyA) that  
614 were NOT stranded. This means that the strand of origin of each read is unknown. To  
615 address this uncertainty, the complement AND reverse complement of both R1 and R2  
616 were concatenated into the final FASTQ file. As described below in the section  
617 “Processing of short-read short-RNAseq (total) and short-RNAseq (polyA) span files”,  
618 future processing kept the most-likely alignment strand for each read.

619

## 620 **Sequence Alignment and Processing**

621 Most long-read sequencing data and Illumina sequencing data were aligned to the  
622 appropriate viral genome using Minimap2 (Li, 2018). The exceptions are the short-  
623 RNAseq (total) JCPyV data from Assetta et al. (Assetta et al., 2016) and the HPyV7  
624 data from Rosenstein et al. (Rosenstein et al., 2021) - these samples contained  
625 sequencing reads of 101bp or shorter and were instead mapped with STAR (Dobin et  
626 al., 2013). All non-primary alignments were discarded. Sequence alignments in BAM  
627 format were then converted to BED using bedtools (Quinlan and Hall, 2010). Here,  
628 bedtools considers any Minimap2- or STAR-called intron (“N” cigar flag) as an intron to  
629 split alignment segments. Parameters for alignment and bed conversion can be found in  
630 `minimap2.sh` and `star.sh`.

631

632 To capture transcripts that originate from a pre-mRNA that circled the viral genome  
633 more than once, and therefore contain repetitive sequences, all alignments were  
634 conducted against concatenated copies of the viral genome. In the case of short-read  
635 short-RNAseq (total) and short-RNAseq (polyA), the reference consisted of two  
636 concatenated copies of the viral genome. For long-read dRNAseq and SMRTseq, the  
637 reference consisted of twenty concatenated copies of the viral genome.

638

639 Because the references consisted of multiple copies of the same viral genome, mapped  
640 reads were assigned to a random copy of the genome. Therefore, all reads in resultant  
641 BED files were “slid” such that they started in the first genome copy of the reference  
642 using `bed_slide_wraparound_reads.py`.

643

644 All reference genomes can be found in `resources/ref` directory of the associated github  
645 repository. All references used contain the PyV late region at the start/5' end of the  
646 reference on the “+” or sense strand, with the early region on the antisense or “-“ strand.  
647 The concatenated references are based on the following reference genomes collected  
648 from NCBI, with any modifications listed:

- 649 - SV40: NC\_001669.1. The first 100 nucleotides were moved to the end of the  
650 sequence.
- 651 - BKPyV: KP412983.1
- 652 - JCPyV: NC\_001699.1

653 - MPyV: NC\_001515.2. The sequence was reverse-complemented to orient the  
654 late region towards the start of the reference.

655 - MCPyV: NC\_010277.2

656 - HPyV7: NC\_014407.1

657 - BSPyV1: LN846618.1

658

659 Next, a span file was generated from each slid BED file using `bed_to_span.py`. This  
660 script splits each read into “spans”, where each span is an exon or an intron with all  
661 positions relative to the viral genome. The introns are defined by the Minimap2- or  
662 STAR-called introns (“N” cigar flag) as mentioned above. All regions between the start  
663 and end of the reads that are not introns were called as distinct exons. Transcripts were  
664 clustered into transcript classes based on introns as discussed below. A “tidy” output  
665 span file was then generated that contains the name, strand, and transcript class of a  
666 given read, with separate lines for the start and end of each span (e.g., exon or intron)  
667 within the sequencing read.

668

### 669 **Alignment of repetitive regions**

670 Reads that originate from a transcript that circles the genome more than once can be  
671 detected because there is one or more repetitive regions within the read. Alignment  
672 against multi-copy reference genomes (20 copies in the case of dRNAseq and  
673 SMRTseq) as described above sufficiently captured most of these transcripts, with  
674 some exceptions. First, BKPyV SMRTseq data had a poor alignment rate of the leader

675 exon in late WA transcripts - this means that WA transcripts are underrepresented in the  
676 BKPyV SMRTseq data. Second, alignment of superT and superT\* transcripts from  
677 SMRTseq and dRNAseq data was generally poor, with the repetitive region often failing  
678 to map via Minimap2. Potential superT and superT\* reads in dRNAseq and SMRTseq  
679 data were identified through assessment of BAM files following mapping. Early reads  
680 that contain a CIGAR flag showing an insertion of 100 bases or more were flagged, and  
681 up to 50 of these transcripts were manually investigated through online BLASTN  
682 (Johnson et al., 2008) against the viral reference genome. Reads supporting superT in  
683 SV40 dRNAseq data, superT\* in SV40 SMRTseq data, and superT in BKPyV SMRTseq  
684 data were initially missing from Minimap2 alignments but were identified via this  
685 approach. One transcript of each type was then repaired upon data import to R such  
686 that these transcripts are represented in downstream visualizations - these actions are  
687 clearly marked in UTILS\_import\_data.R. Thus, superT and superT\* in SMRTseq and  
688 dRNAseq data are underrepresented in abundance plots (**Figure S3D, S4D**) and read  
689 pileups (**Figure S6, S8**) compared to their actual abundance in the cell due to these  
690 alignment challenges.

691

## 692 **Generation of transcript classes**

693 Transcript classes were generated during processing of BED files using  
694 bed\_to\_span.py. Each transcript class consists of sequencing reads that contain the  
695 same combination of introns. The transcript class number is based on the abundance of  
696 transcripts within a transcript class - e.g., transcript class 1 contains more transcripts  
697 than transcript class 2, and so on. Transcript class generation is similar for both long-

698 and short-read sequencing data, although short reads usually (but not always) tend to  
699 contain a maximum of one intron. Notably, transcript class assignment is independent of  
700 the transcript start and end positions, meaning that there can be heterogeneity of  
701 transcript start and end positions within a transcript class. For all SMRTseq and  
702 dRNAseq data, for a transcript class to be generated all introns contained within the  
703 transcript class were required to be supported by at least 5 junction-spanning reads  
704 within a short-RNAseq (total) dataset. For SV40 and BKPyV Dunlop SMRTseq and  
705 dRNAseq data, the short-RNAseq (total) data was generated from RNA from the same  
706 extraction. SV40 dRNAseq replicate 2 was corrected with the short-RNAseq (total) data  
707 from the first SV40 replicate. For the MPyV dRNAseq data, short-RNAseq (total) data  
708 from Garren et al. was used. If a transcript contained an intron that was not supported  
709 by at least 5 junction-spanning reads in the Illumina dataset, it was discarded. We opted  
710 to use this filtering strategy rather than implementing long-read correction because  
711 correction algorithms were unable to cope with wraparound transcripts.

712

713 There were limited circumstances where dRNAseq or SMRTseq transcript classes were  
714 removed manually during processing - this occurred to four transcript classes that made  
715 it through filtering. In these circumstances, alignments were deemed to be artifactual  
716 due to Minimap2 alignment errors. These instances are clearly programmatically  
717 marked in UTILS\_import\_data.R with specific rationale for each action.

718

719 **Splice coordinate system**

720 All splice or intron positions marked in any figure or table of this manuscript are **0-**  
721 **indexed positions of the intron**. To convert these coordinates to the 1-  
722 indexed/absolute position of the intron on the viral genome, add 1 to the intron start  
723 position. For example, for the intron 276-1600, viral genome nucleotide # 277 is the first  
724 nucleotide within the intron, and viral genome nucleotide # 1600 is the last nucleotide  
725 within the intron.

726

### 727 **Processing of short-RNAseq (total) and short-RNAseq (polyA) span files**

728 The majority of the short-read RNAseq data investigated here used a strand-specific  
729 sequencing strategy (except for the MCC tumor RNAseq). With this strategy, the strand  
730 of origin for the transcript yielding each read is known, and a read can be correctly  
731 assigned to the sense (“+” / late) or antisense (“-“ / early) strand. However, a fraction of  
732 transcripts can be inaccurately stranded due to artifacts during library preparation.  
733 When there were many more late reads than early reads in a short-read dataset, a  
734 prohibitive fraction of “early” reads would be reads from late transcripts that were  
735 incorrectly stranded due to this artifact. To address this issue, short reads that aligned  
736 to the + strand were required to either start or end within the late region (defined as the  
737 first ½ of the genome), and short-reads that aligned to the - strand were required to  
738 either start or end within the early region (defined as the second ½ of the genome).

739

### 740 **Transcript identification**



741 For **Figure 1** and all supplementary figures, a SV40 or BKPyV transcript was identified  
742 and assigned a transcript ID if it was at least 0.1% of early or late strands in dRNAseq  
743 or SMRTseq data with one exception - SV40 transcript L8 had been previously  
744 identified and was kept despite being at only 0.06% abundance. Existing transcript  
745 names, where available, were taken from relevant studies (Abend et al., 2009; Good et  
746 al., 1988; Seif et al., 1979; Zerrahn et al., 1993). This assignment occurred from the  
747 span files, meaning that all sequencing reads in question were previously required to  
748 contain introns that were supported by at least 5 short-RNAseq (total) junction-spanning  
749 reads. For SV40, for which there was two dRNAseq replicates, identification of a  
750 sequencing read at 0.1% or greater in just one replicate was sufficient.

751

752 Transcript IDs (e.g., E1, E2, E3..., L1, L2, L3,...) consist of the kinetic class (E: Early, or  
753 L: Late) of the identified transcript followed by an integer value in ascending order of  
754 abundance. This abundance value was calculated by ordering the transcripts in order of  
755 the maximum observed relative abundance in dRNAseq or SMRTseq data.

756

757 Of note, the relative abundance of transcripts between dRNAseq and SMRTseq data is  
758 skewed by distinct read-length biases between the two approaches. The dRNAseq  
759 approach has a 3' bias and a bias towards shorter transcripts, while SMRTseq library  
760 preparation resulted in preferential sequencing of transcripts closer to ~2500bp in  
761 length. Resultant differences in the length of aligned reads can be seen in **Figure S1C**.

762 The TSS distribution of SV40 late transcripts varies between transcript classes, while

763 the late TSS distribution tends to be similar across transcript classes in BKPyV (**Figure**  
764 **S2A**).

765

#### 766 **Calculation of sequencing coverage**

767 To determine the sequencing coverage for each sample (as in **Figure 1C**), BAM files  
768 from alignment were “slid” such that all transcripts must start in the first genome copy of  
769 the reference using `bam_slide_wraparound_reads.py`, in a similar manner as the beds  
770 were slid as described above. Forward and reverse strand reads were split, and the  
771 depth was calculated using the command ``samtools depth -aa -d0`` separately for  
772 forward and reverse reads. These processing steps are present in `bam_coverage.nf`.  
773 During plotting, the coverage for each strand was normalized to the maximum coverage  
774 at any position (e.g., the maximum coverage of the late and early strands was set to 1).

775

#### 776 **Watch plots**

777 Each panel of a watch plot represents information for a single transcript class. The  
778 center “arms” of these plots are histograms detailing the distribution of start (blue) and  
779 end (red) positions for the transcripts within the transcript class. These histograms are  
780 normalized to the highest abundance position. The outer ring of each watch plot shows  
781 the viral ORF map. Each inner grey ring indicates the number of genomes spanned - all  
782 transcripts are displayed moving outwards from the center. Red segments indicate the  
783 **exons** of each transcript class. The first exon starts on the most-inner grey ring at the  
784 most common transcript start site for the transcript class, and the last exon ends on the

785 most-outer grey ring at the most common transcript end site for the transcript class. The  
786 3' end of the transcript is indicated by the red arrow at the end of the last exon. Thus,  
787 the transcripts spiral outwards from the center in the direction of the red arrow. **Figure 4**  
788 contains a schematic key describing watch plots.

789

### 790 **Read pileup plots**

791 Each square/rectangular panel of a read pileup plot shows the reads present in a single  
792 transcript class. The arrows at the top of each panel indicate the viral ORF map, with  
793 dashed lines indicating the end of each genome copy. Next, the lines indicate  
794 histograms of the transcript start (blue) and end (red) sites for the transcripts within the  
795 transcript class. Below the x-axis, each row indicates a single sequencing read. The  
796 spans in red indicate the exons inferred from a sequencing read, while the spans in pink  
797 indicate the introns/splice junctions. Sometimes the distribution of transcript end  
798 positions for a transcript class can be obscured by the thickness of the transcript lines -  
799 the histograms should always be consulted to assess abundance.

800

801 For SV40 dRNAseq watch and pileups: There were two SV40 dRNAseq replicates.  
802 Watch plots and read pileups are based on replicate 1, although missing transcripts that  
803 were identified in replicate 2 but not 1 were also plotted.

804

### 805 **Short-read intron plots (Figure S9, S11)**

806 In these plots, lines indicate specific introns. The upper and lower horizontal arrows  
807 indicate the viral ORF map - often, these ORF maps will indicate two concatenated viral  
808 reference genomes. The circles above or below each ORF map indicate the percentage  
809 of early or late introns that fall at each genome position. Early introns and percentages  
810 are colored red, while late introns and percentages are colored blue.

811

## 812 **polyA tail length**

813 polyA tail length was determined from dRNAseq data using the `polya` command of  
814 Nanopolish (Loman et al., 2015). To determine the polyA distribution of host transcripts,  
815 sequencing reads were aligned to the human GRCh38 (for BKPyV samples), *C.*  
816 *Sabaeus* (for SV40 samples), or mouse (for MPyV) cDNA transcriptomes downloaded  
817 from ensembl. Only reads with a Nanopolish QC tag of “PASS” were considered for  
818 downstream polyA tail length analyses.

819

820 The dRNAseq library preparation included the addition of the “RNA Control Standard”  
821 (RCS), which is a synthetic RNA based on yeast ENO2 containing a 30-adenine polyA  
822 tail. dRNAseq samples were mapped against ENO2 to assess the polyA tail length  
823 distribution of this control.

824

825 The cumulative incidence of transcript termination (**Figure S10D**) was calculated by  
826 determining, for each early read, how far the read's transcript end site is from the  
827 canonical polyA site position for each virus.

828

### 829 **Polysome profiling analysis**

830 To determine the ribosome occupancy of host genes, dRNAseq reads were aligned to  
831 the *C. Sabaeus* cDNA transcriptome downloaded from ensembl. The number of reads  
832 mapped to each transcript was extracted with `samtools idxstats`. Transcripts were  
833 filtered to include only those with at least 10 reads in both polysome and input fractions.  
834 The normalized abundance of each transcript in each fraction was defined as (# of  
835 mapped reads)/(total number of virus and host mapped reads). Ribosome occupancy of  
836 each transcript was determined as (normalized abundance in polysome)/(normalized  
837 abundance in whole-cell), where a value of >1 indicates preferential translation.

838

839 Ribosome occupancy of individual viral transcripts could not be calculated because of  
840 increased rates of transcript truncation in the polysome fraction compared to the whole-  
841 cell fraction. This was indicated by a nearly doubled proportion of unspliced reads with  
842 premature 5' ends in the polysome fraction compared to the whole-cell fraction, and  
843 likely indicates transcript degradation during sucrose centrifugation or fraction collection.  
844 Because viral transcripts are mostly identical and vary largely at a 5' splice site,  
845 elevated transcript truncation decreased the observed abundance of individual viral

846 transcripts in the polysome fraction and make ribosome occupancy calculations for  
847 individual viral transcripts unreliable.

848

#### 849 **MCC440 superT PCR and sanger sequencing**

850 Anchored poly-dT primers (Life Technologies) were used for specific reverse-  
851 transcription of full-length mRNA into cDNA. Primers were designed to uniquely amplify  
852 the super-LT junction through exploitation of repetitive sequences. Primer sequences  
853 were as follows (5' -> 3'); Forward: CTGGACTGGGAGTCTGAAGC, Reverse:  
854 ACCCCTCCTCCATTCTCAAGA. Q5 polymerase (NEB) with standard reaction  
855 conditions was used for amplification.

856

#### 857 **Generation of integrated PyV structures and viral variant calling**

858 Tumor WGS was aligned against a fusion reference genome containing hg38 and  
859 Merkel cell polyomavirus (NC\_010277) using bowtie2 with default parameters.  
860 Integrated virus assembly graphs and annotations were generated using Oncovirus  
861 tools ([https://github.com/gstarrett/oncovirus\\_tools](https://github.com/gstarrett/oncovirus_tools)). Assembly graphs were then  
862 manually interpreted to create linear integration structures for PyV-associated MCC.

863

864 Point mutations were called in the PyV genomes using lofreq with default parameters  
865 (<https://csb5.github.io/lofreq/>) (PMID: 23066108). Lofreq output was functionally  
866 annotated with SnpEff (<http://pcingola.github.io/SnpEff/>) (PMID: 22728672) using the

867 relevant GenBank gene annotations for the above genomes. Variants were plotted out  
868 in R with the ggplot2 package.

869

870

## 871 List of abbreviations

872 APA - Alternative polyadenylation

873 BKPyV - BK Polyomavirus

874 BSPyV1 - Bark scorpion polyomavirus 1

875 dRNAseq - Nanopore direct RNA sequencing

876 HPyV7 - Human polyomavirus 7

877 JCPyV - JC Polyomavirus

878 LT - Large T antigen

879 MCC - Merkel cell carcinoma

880 MCPyV - Merkel cell polyomavirus

881 MPyV - Murine polyomavirus

882 MT - Middle T antigen

883 ORF - Open reading frame

884 SMRTseq - PacBio SMRT sequencing

885 ST - Small T antigen

886 SV40 - Simian virus 40

887 TES - Transcript end site

888 TSS - Transcript start site

889 PVAN - Polyomavirus-associated nephropathy

890 PyV - Polyomavirus

891

892

## 893 **Declarations**

### 894 **Competing interests**

895 M.M. receives research support from Bayer, Janssen, Ono; consults for Bayer, Interline,  
896 Isabl; and receives patent royalties from Labcorp and Bayer. J.A.D. has received  
897 research support from Rain Therapeutics, Inc. and is a consultant for Rain  
898 Therapeutics, Inc. and Takeda, Inc.

899

### 900 **Funding**

901 This work was supported in part by the US Public Health Service grants R35CA232128  
902 and P01CA203655 and by the Bridge Project, a partnership between the Koch Institute  
903 for Integrative Cancer Research at MIT and the Dana-Farber/Harvard Cancer Center to



904 J.A.D.; a Cancer Grand Challenges OPTIMISTIC team award (C10674/A27140) and  
905 by National Cancer Institute grant R35CA197568 to M.M.; R01 AI060584 and R21  
906 AI147155 to M.J.I.; CD & SV were supported by R35GM134944; GJS is supported by  
907 the NIH Intramural Research Program.

908

### 909 **Authors' Contributions**

910 Conceptualization - J.N., M.M., J.A.D.

911 Data curation - J.N.

912 Formal analysis - J.N.

913 Funding acquisition - M.M., J.A.D., M.J.I., S.V., G.J.S.

914 Investigation - J.N., W.Z., T.C.F., C.D.

915 Methodology - J.N., M.M., J.A.D.

916 Project administration - J.N.

917 Resources - J.N., M.M., J.A.D., T.C.F., W.Z., M.J.I., S.V., C.D.

918 Software - J.N.

919 Supervision - M.M., J.A.D.

920 Validation - J.N.

921 Visualization - J.N.

922 Writing, Original draft - J.N., M.M., J.A.D.

923 Writing, review & editing - J.N., W.Z., T.C.F., C.D., S.V., G.J.S., M.J.I., M.M., J.A.D.

924

## 925 **Acknowledgements**

926 We thank Katie Vicari ([www.KatieRisVicari.com](http://www.KatieRisVicari.com)) for her work illustrating Figure 1A, 2, 3,  
927 and S12B. Figure 1F was made in BioRender. We thank Mary O'Reilly with the Broad  
928 Research Communication Lab for helpful discussions on figure design. We thank  
929 Robert Garcea and Kimberly Erickson for kindly providing stocks of MPyV. Portions of  
930 this research were conducted using the O2 High Performance Computing Cluster,  
931 supported by the Research Computing Group at Harvard Medical School. Portions of  
932 this work utilized the computational resources of the NIH HPC Biowulf cluster  
933 (<http://hpc.nih.gov>).

934

## 935 **Figure legends**

936 **Figure 1** - RNA sequencing expands known SV40 and BKPyV transcript diversity.

937 **A.** Overview of experimental procedures. Cells were infected with a polyomavirus,  
938 and RNAs extracted. RNA was sequenced using long-read (Nanopore dRNAseq  
939 and PacBio SMRTseq) and short-read (Illumina short-RNAseq (total) and short-  
940 RNAseq (polyA)). Transcripts were analyzed, and the impact of observed splice  
941 events on viral open reading frames was assessed.

942 **B.** Mechanism of transcript clustering in this study. Transcripts were aligned to the  
943 viral genome and grouped into transcript classes based on the presence of

944 shared introns. Thus, within a transcript class there may be variation in the exact  
945 transcript start and end positions. This clustering strategy was used for both long-  
946 and short-RNAseq data.

947 **C.** Viral RNA sequence coverage for SV40 and BKPyV as determined from  
948 dRNAseq, SMRTseq, and short-RNAseq (total) data. The Y axis indicates the  
949 scaled coverage, with X axis indicating the position on the viral genome.  
950 Coverage for late transcripts (mapping to the + strand) is above the x axis, while  
951 coverage for early transcripts (mapping to the - strand) is below the x axis.  
952 Coverage is scaled separately for each strand such that the maximum observed  
953 coverage for each strand is 1. Arrows at the top of the plot indicate the positions  
954 of viral genes.

955 **D-E.** UpSet plot indicating the overlap between existing transcript annotations,  
956 dRNAseq data, and SMRTseq data for SV40 (**D**) and BKPyV Dunlop (**E**). Bars  
957 indicating overlap with existing transcript annotations are black, while those  
958 indicating no overlap with existing annotations are blue. These blue bars indicate the  
959 number of novel, unannotated transcripts identified.

960 **F.** Overview of polysome profiling of SV40-infected cells. BSC40 cells were  
961 infected with SV40. Cells were lysed, and a portion of the lysate was subjected to  
962 dRNAseq (representative of the RNA content of the whole cell). The remaining  
963 lysates was centrifuged through a sucrose gradient, after which fractions  
964 containing RNA associated with two or more ribosomes were pooled and  
965 subjected to dRNAseq.

966 **G.** Relative abundance of SV40 early and late transcripts in the whole-cell and  
967 polysome fractions of SV40-infected cells. Y-axis indicates the percentage of  
968 early or late transcripts and is log scale. X axis indicates each transcript, with  
969 black dots indicating each transcript's whole-cell relative abundance and red dots  
970 indicating each transcript's polysome relative abundance.

971

972 **Figure 2** - Annotated and novel SV40 transcripts.

973 **A.** Transcripts are shown relative to the viral genome. Each line is a viral transcript,  
974 with red lines indicating exons and dashed blue lines indicating introns. Spokes  
975 indicate the positions of common splice donors and splice acceptors. Transcripts  
976 that were annotated prior to this study are on a yellow background, and novel  
977 transcripts are on a white background. Wraparound transcription that results in  
978 multiple copies of a region is annotated with double lines, and the number of  
979 copies is indicated in parentheses. The line labeled "pA" indicates the  
980 approximate position of the polyA signal sequence.

981 **Figure 3** - Annotated and novel BKPyV transcripts.

982 **A.** Transcripts are shown relative to the viral genome. Each line is a viral transcript,  
983 with red lines indicating exons and dashed blue lines indicating introns. Spokes  
984 indicate the positions of common splice donors and splice acceptors. Transcripts  
985 that were annotated prior to this study are on a yellow background, and novel  
986 transcripts are on a white background. Wraparound transcription that results in  
987 multiple copies of a region is annotated with double lines, and the number of

988 copies is indicated in parentheses. The line labeled “pA” indicates the  
989 approximate position of the polyA signal sequence.

990

991 **Figure 4** - Pervasive wraparound transcription across PyV

992 **A-C.** Watch plots indicating the top 4 highest abundance late wraparound  
993 transcript classes in dRNAseq data from SV40 (A), BKPyV Dunlop (B), and  
994 MPyV (C). The outer ring of each watch plot indicates the position of the viral  
995 ORFs. The inner arms are histograms detailing the distribution of transcript starts  
996 (in blue) and ends (in red) for transcripts within each transcript class. The red  
997 segments indicate exons. Transcripts start in the innermost ring - a second or  
998 third ring indicates that the pre-mRNA that generated the transcript must have  
999 circled the viral genome multiple times. The 3' end of the transcript and the  
1000 direction in which these plots are oriented is indicated by the red arrow at the end  
1001 of the last exon segment. The red exon segments start at the most common  
1002 transcript start site within the transcript class, and end at the most common  
1003 transcript end site within the class. The watch plot key shows an example of the  
1004 path of the pre-mRNA for SV40 transcript class L6\_I.

1005 **D.** Bar plots indicating the percentage of late transcripts that span a given number of  
1006 genome lengths in SV40, BKPyV Dunlop, and MPyV dRNAseq data.

1007 **E.** The leader-leader junction, that connects the pre-mRNA from one genome to the  
1008 subsequent wraparound, was identified in Illumina short-RNAseq (total) data.

1009 The intron in question is plotted as a black line in this plot, with the x axis

1010 indicating the genomic position of the intron. The top late wraparound transcript  
1011 for each virus was plotted. The gene map indicates the approximate gene  
1012 position and is accurate for SV40 - the exact position of the viral genes varies  
1013 between viruses. Percentages indicate the percentage of late junction-spanning  
1014 transcripts that support the plotted wraparound leader-leader junction.

1015 **F.** Schematic illustrating how leader-leader wraparound transcription can be  
1016 detected from short read short-RNAseq (total). Leader-leader splicing can be  
1017 seen as a repetitive exon in watch plots from long-read RNAseq data. Ultimately,  
1018 there was an original processed mRNA in the cell that contained two tandem  
1019 leader sequences. When this transcript of origin is sequenced via short read  
1020 sequencing, reads will be generated across its length. A minority of these reads  
1021 will span the leader-leader junction, and mapping against the viral reference  
1022 genome can be used to uncover leader-leader splicing.

1023 **Figure 5** - Detection of novel, conserved splicing events that expand PyV coding  
1024 capacity.

1025 **A-D.** Schematics illustrating identified ORFs. Each row is a reading frame (except for  
1026 ST and the LT 1<sup>st</sup> exon, which are in the same frame), and unannotated amino acids are  
1027 represented by grey boxes. The measured intron is indicated by the red arrow. Colored  
1028 ORFs are annotated, while grey ORFs are unannotated. Percentages on the right side  
1029 of the figure are the percentage of spliced viral transcripts on the same strand as  
1030 determined from short-read short-RNAseq (total) data. Numbers after each virus name  
1031 indicate the transcript class within each short-RNAseq (total) dataset. The measured  
1032 intron is indicated by the red arrow.

1033 A) ST2: This ORF is generating from a splicing event that uses the LT first exon  
1034 donor and an acceptor within the ST ORF. In HPyV7 and BKPyV Dunlop, the splice  
1035 lands in frame and results in an internal deletion within ST. In MPyV and MCPyV the  
1036 splice lands out of frame, resulting in an ORF that contains the N-terminal region of  
1037 ST and novel amino acids at the C terminus.

1038 B) MT: MPyV encodes a MT following splicing connecting the end of the ST ORF  
1039 with an ORF in an alternate frame of the LT second exon. In BKPyV, a similar splice  
1040 occurs connecting ST with an MT-like ORF in an alternative frame of the LT second  
1041 exon.

1042 C) VP1X: JCPyV encodes two VP1X ORFs generated by splicing within VP1 and  
1043 landing in an alternative frame of VP1, or earlier in the late region due to wraparound  
1044 transcription. While predominant in JCPyV, VP1X is likewise present in many other  
1045 PyV.

1046 D) superT: The superT-specific splice utilizes the splice donor canonically  
1047 associated with truncated T antigens such as 17kT in SV40 and truncT in BKPyV.  
1048 Due to wraparound transcription, a LT second exon acceptor is available to the 3' of  
1049 this donor and acts as the acceptor. For the superT ORF to form, an initial LT splice  
1050 is required. Ultimately, superT contains a duplication in part of the LT second exon  
1051 that includes the RB-binding LxCxE motif.

1052 **E.** Schematics detailing BKPyV Dik isolates used for querying the existence of superT.  
1053 BKPyV WT is wild type virus. M1 contains a LT intron that has been replaced with an  
1054 intron from the plasmid pCI. Both WT and M1 are expected to generate LT and superT

1055 of expected sizes. M2 has a completely removed LT intron, and the pCI intron is located  
1056 directly 5' of the LT ORF. M2 is expected to encode LT of expected size, but a larger  
1057 superT variant due to incorporation of a second copy of the LT first exon.

1058 **F.** Western blot of cells infected with BKPyV Dik WT, M1, or M2 and probed with an  
1059 antibody reactive against LT. The lower molecular weight band is LT, and the higher  
1060 molecular weight bands are consistent with superT.

1061

1062 **Figure 6** - Detection superT-encoding transcripts in PyV-associated cancers

1063 **A.** Schematic detailing the generation of superT during lytic infection as compared  
1064 to from integrated virus in cancer. During viral infection, the RNA polymerase can  
1065 circle the viral genome multiple times, resulting in a pre-mRNA that can be  
1066 spliced to generate superT. In the case of host integration, a polyomavirus can  
1067 be integrated in tandem copies such that a pre-mRNA is generated with more  
1068 than one copy of the viral early region. This pre-mRNA can be similarly spliced to  
1069 generate a superT transcript.

1070 **B.** Heatmap indicating the abundance of the superT, ST, and LT introns from  
1071 RNAseq data from two replicates of a BKPyV-positive bladder cancer and six  
1072 MCPyV-associated MCCs. Percentages indicate the percentage of spliced early  
1073 viral reads for each sample. The splice measured in each row is indicated by the  
1074 red arrow in the schematics on the right side of the figure.

1075

1076 **Figure S1** - Sequencing statistics



1077 **A.** The number of reads for all datasets studied here. For long-read dRNAseq and  
1078 SMRTseq, this number includes spliced and unspliced reads. Because short  
1079 reads are only useful for transcript characterization when they span a splice  
1080 junction, the counts for short-reads represent the number of splice-junction-  
1081 spanning reads.

1082 **B.** The cumulative percentage of transcripts in each number of transcript classes, by  
1083 strand. The X-axis indicated the total number of transcript classes. The Y axis  
1084 indicates the cumulative percentage of transcripts within those transcript classes.  
1085 These plots indicate that most transcripts in most samples are contained within  
1086 the first few transcript classes.

1087 **C-E.** The alignment length distribution of early, late, spliced, and unspliced  
1088 transcripts for dRNAseq and SMRTseq data from SV40 (**C**), BKPyV Dunlop (**D**), and  
1089 MPyV (**E**). The X axis indicates the length of a read's alignment, while the Y axis  
1090 indicates the density/percentage of transcripts with a given alignment length. This  
1091 plot shows that dRNAseq and SMRTseq data sample from RNA populations of  
1092 different length.

1093

1094 **Figure S2** - Transcript start sites and polyA tail lengths.

1095 **A, B.** The distribution of transcript start sites for late (**A**) and early (**B**) transcripts for  
1096 SV40 (left column), BKPyV Dunlop (middle column), and MPyV (right column). The  
1097 arrows indicate the viral ORF positions.

- 1098        **C.** The distribution of polyA tail lengths for the 30-adenine ENO2 control (black),  
1099            host (red), and viral (yellow) transcripts for SV40, BKPyV Dunlop, and MPyV.  
1100            The X axis indicates the length of the polyA tail, while the Y axis indicates the  
1101            density/percentage of transcripts with each length.
- 1102        **D.** Ribosome occupancy of host transcripts in SV40-infected cells. Each grey dot is  
1103            a host transcript. The red, blue, and black dots are specifically noted host  
1104            transcripts. Ribosome occupancy is on the Y axis, while the X axis does not hold  
1105            value. Lines on the violin plot indicate 1<sup>st</sup>, 2<sup>nd</sup>, and 3<sup>rd</sup> quartiles.

1106

1107    **Figure S3** - SV40 transcriptome atlas, watch plots

- 1108            **A-C.** Watch plots indicating all identified transcripts in SV40. **(A)** and **(B)** show  
1109            transcripts that were identified in both dRNAseq and SMRTseq data, while **(C)**  
1110            shows transcripts identified in SMRTseq only.

- 1111        **E.** Barplots that show the abundance of each transcript type in the dRNAseq and  
1112            SMRTseq data. Here, there are two dRNAseq bars (one per replicate). The Y  
1113            axis indicates the percentage of transcripts of the same strand. As discussed in  
1114            the methods, alignment of superT and superT\* was challenging, so the actual  
1115            abundance of these transcripts is higher than reported here.

1116

1117    **Figure S4** - BKPyV Dunlop transcriptome atlas, watch plots

1118 **A-C.** Watch plots indicating all identified transcripts in BKPyV Dunlop. **(A)** and  
1119 **(B)** show transcripts that were identified in both dRNAseq and SMRTseq data,  
1120 while **(C)** shows transcripts identified in dRNAseq only.

1121 **F.** Barplots that show the abundance of each transcript type in the dRNAseq and  
1122 SMRTseq data. The Y axis indicates the percentage of transcripts of the same  
1123 strand. As discussed in the methods, alignment of superT and superT\* was  
1124 challenging, so the actual abundance of these transcripts is higher than reported  
1125 here.

1126

1127 **Figure S5** - SV40 transcriptome atlas, late transcript read pileups

1128 **A, B.** Read pileups showing the late transcripts identified in SV40 dRNAseq (A)  
1129 and SMRTseq (B). The arrows at the top of the plot indicate the viral ORF  
1130 positions. Below the X axis, each row is an individual transcript, with exons  
1131 indicated in red and splice junctions/introns indicated in pink. Above the X axis  
1132 are histograms indicating the transcript start (blue) and transcript end (red) sites.  
1133 (U: unspliced).

1134

1135 **Figure S6** - SV40 transcriptome atlas, early transcript read pileups

1136 **A, B.** Read pileups showing the early transcripts identified in SV40 dRNAseq (A)  
1137 and SMRTseq (B). The arrows at the top of the plot indicate the viral ORF  
1138 positions. Below the X axis, each row is an individual transcript, with exons

1139 indicated in red and splice junctions/introns indicated in pink. Above the X axis  
1140 are histograms indicating the transcript start (blue) and transcript end (red) sites.  
1141 (U: unspliced).

1142

1143 **Figure S7** - BKPyV Dunlop transcriptome atlas, late transcript read pileups

1144 **A, B.** Read pileups showing the late transcripts identified in BKPyV Dunlop  
1145 dRNAseq (A) and SMRTseq (B). The arrows at the top of the plot indicate the  
1146 viral ORF positions. Below the X axis, each row is an individual transcript, with  
1147 exons indicated in red and splice junctions/introns indicated in pink. Above the X  
1148 axis are histograms indicating the transcript start (blue) and transcript end (red)  
1149 sites. (U: unspliced).

1150

1151 **Figure S8** - BKPyV Dunlop transcriptome atlas, early transcript read pileups

1152 **A, B.** Read pileups showing the early transcripts identified in BKPyV Dunlop  
1153 dRNAseq (A) and SMRTseq (B). The arrows at the top of the plot indicate the  
1154 viral ORF positions. Below the X axis, each row is an individual transcript, with  
1155 exons indicated in red and splice junctions/introns indicated in pink. Above the X  
1156 axis are histograms indicating the transcript start (blue) and transcript end (red)  
1157 sites. (U: unspliced).

1158

1159 **Figure S9** - Intron plots for all datasets studied

- 1160 A. Intron plots generated from short-read RNAseq. The arrows at the top and  
1161 bottom of each panel indicate the position of viral ORFs. The lines indicate  
1162 specific introns identified in the RNAseq data, with the 5' end on the top and the  
1163 3' end on the bottom. The blue color indicates late transcripts, with red indicating  
1164 early transcripts. The size of the circles above and below the viral ORF maps  
1165 indicate the percentage of junction-spanning reads with a 5' end (on top) or 3'  
1166 end (on bottom) at that position. Junctions are plotted if they are at least 1% of  
1167 early or late transcripts, except for the SV40 pA superT junction (transcript class  
1168 3) which is just below threshold but is of interest.
- 1169 B. Another representation of intron plots for each virus. The top arrows indicate the  
1170 position of viral ORFs. The X axis indicates the genomic position for each splice.  
1171 The Y axis indicates a single transcript class, with that class' intron plotted as a  
1172 line. The percentage of early or late transcripts is indicated with the numeric  
1173 percentage. Junctions are plotted if they are at least 1% of early or late  
1174 transcripts, except for the SV40 pA superT junction (transcript class 3) which is  
1175 just below threshold but is of interest.

1176

1177 **Figure S10** - Alternative polyadenylation of early transcripts in SV40, BKPyV, and  
1178 MPyV.

1179 **A-C.** Watch plots indicating the LT and ST transcripts for SV40 (**A**), BKPyV  
1180 Dunlop (**B**), and MPyV (**C**). The focus of these plots is the distribution of  
1181 transcript end positions, which are the inner red arms. The region of APA of  
1182 highlighted in blue, with the canonical transcript end sites highlighted in red.

1183 **D.** A cumulative incidence plot of transcript termination in SV40 (blue), BKPyV  
1184 Dunlop (red), and MPyV (green). The X axis indicates the distance to the  
1185 canonical polyA site, while the Y axis indicates the percentage of transcripts that  
1186 have terminated by that position.

1187 **E-G.** Density plots showing the distribution of polyA tail lengths for LT and ST  
1188 transcripts that end at the canonical site (solid) or undergo APA (dashed) for  
1189 SV40 (**E**), BKPyV Dunlop (**F**), and MPyV (**G**). The x axis indicates the length of  
1190 the polyA tail, while the Y axis indicates the density/proportion of transcripts with  
1191 the given length.

1192

1193 **Figure S11** - short-RNAseq (polyA) analysis of BKPyV Dik WT, M1, and M2

1194 **A-C.** Intron plots generated from short-read (polyA) RNAseq of cells infected with  
1195 BKPyV WT, or the M1 or M2 mutants. The arrows at the top and bottom of each panel  
1196 indicate the position of viral ORFs relative to the standard BKPyV genome - note that  
1197 the genomes of mutants M1 and M2 are altered as indicated in Figure 5E. The lines  
1198 indicate specific introns identified in the RNAseq data, with the 5' end on the top and the  
1199 3' end on the bottom. The size of the circles above and below the viral ORF maps  
1200 indicate the percentage of junction-spanning reads with a 5' end (on top) or 3' end (on  
1201 bottom) at that position. Only early junctions that are at least 1% of early early  
1202 transcripts are plotted. The superT junction is colored in gold. (**A**) Intron plot for BKPyV  
1203 Dik WT. (**B**) Intron plot for BKPyV Dik M1. (**C**) Intron plot for BKPyV Dik M2.

1204

1205 **Figure S12 - superT in MCPyV-associated MCC**

- 1206 A. Sanger sequencing of an RT-PCR product from MCC J45\_440, showing the  
1207 superT-specific junction.
- 1208 B. A schematic detailing the MCC 285 MCPyV integration site, showing how it is  
1209 possible that superT is generated via cis-splicing.
- 1210 C. The assembled viral block in MCC tumor J45\_440. This integration site is based  
1211 on de-novo assembly using short whole genome sequencing reads. Despite only  
1212 assembling one viral block, we found that 1) there are likely 2 copies of the viral  
1213 genome, and 2) the 5' viral integration site appears to fall on chromosome 7  
1214 "after" the 3' viral integration site, observations consistent with the existence of  
1215 two copies of the viral genome in tandem separated by a small segment of host  
1216 DNA at this integration site.
- 1217 D. The assembled viral blocks in MCC tumor J17\_296. The longest block contains  
1218 two copies of the early region.
- 1219 E. Lollipop plots showing identified SNPs in the MCPyV genomes of J45\_440,  
1220 J17\_296, and J11\_285. The gene-map below the figure indicates the position of  
1221 viral ORFs. Each lollipop is colored according to the nucleotide substitution  
1222 identified.

1223

1224

- 1225 Abend, J.R., Joseph, A.E., Das, D., Campbell-Cecen, D.B., and Imperiale, M.J. (2009).  
1226 A truncated T antigen expressed from an alternatively spliced BK virus early mRNA.  
1227 *The Journal of general virology* 90, 1238.
- 1228 Abere, B., Zhou, H., Li, J., Cao, S., Toptan, T., Grundhoff, A., Fischer, N., Moore, P.S.,  
1229 and Chang, Y. (2020). Merkel Cell Polyomavirus Encodes Circular RNAs (circRNAs)  
1230 Enabling a Dynamic circRNA/microRNA/mRNA Regulatory Network. *Mbio* 11, e03059-  
1231 03020.
- 1232 Adami, G., Marlor, C., Barrett, N., and Carmichael, G.G. (1989). Leader-to-leader  
1233 splicing is required for efficient production and accumulation of polyomavirus late  
1234 mRNAs. *Journal of virology* 63, 85-93.
- 1235 Assetta, B., De Cecco, M., O'Hara, B., and Atwood, W.J. (2016). JC polyomavirus  
1236 infection of primary human renal epithelial cells is controlled by a type I IFN-induced  
1237 response. *MBio* 7, e00903-00916.
- 1238 Balázs, Z., Tombácz, D., Szűcs, A., Snyder, M., and Boldogkői, Z. (2017). Long-read  
1239 sequencing of the human cytomegalovirus transcriptome with the Pacific Biosciences  
1240 RSII platform. *Scientific data* 4, 1-7.
- 1241 Carter, J.J., Daugherty, M.D., Qi, X., Bheda-Malge, A., Wipf, G.C., Robinson, K.,  
1242 Roman, A., Malik, H.S., and Galloway, D.A. (2013). Identification of an overprinting  
1243 gene in Merkel cell polyomavirus provides evolutionary insight into the birth of viral  
1244 genes. *Proceedings of the National Academy of Sciences* 110, 12744-12749.



1245 Depledge, D.P., Srinivas, K.P., Sadaoka, T., Bready, D., Mori, Y., Placantonakis, D.G.,  
1246 Mohr, I., and Wilson, A.C. (2019). Direct RNA sequencing on nanopore arrays redefines  
1247 the transcriptional complexity of a viral pathogen. *Nature communications* *10*, 1-13.

1248 Dobin, A., Davis, C.A., Schlesinger, F., Drenkow, J., Zaleski, C., Jha, S., Batut, P.,  
1249 Chaisson, M., and Gingeras, T.R. (2013). STAR: ultrafast universal RNA-seq aligner.  
1250 *Bioinformatics* *29*, 15-21.

1251 Eul, J., and Patzel, V. (2013). Homologous SV40 RNA trans-splicing: a new mechanism  
1252 for diversification of viral sequences and phenotypes. *RNA biology* *10*, 1689-1699.

1253 Freund, R., Sotnikov, A., Bronson, R.T., and Benjamin, T.L. (1992). Polyoma virus  
1254 middle T is essential for virus replication and persistence as well as for tumor induction  
1255 in mice. *Virology* *191*, 716-723.

1256 Garalde, D.R., Snell, E.A., Jachimowicz, D., Sipos, B., Lloyd, J.H., Bruce, M., Pantic, N.,  
1257 Admassu, T., James, P., and Warland, A. (2018). Highly parallel direct RNA sequencing  
1258 on an array of nanopores. *Nature methods* *15*, 201-206.

1259 Garren, S.B., Kondaveeti, Y., Duff, M.O., and Carmichael, G.G. (2015). Global analysis  
1260 of mouse polyomavirus infection reveals dynamic regulation of viral and host gene  
1261 expression and promiscuous viral RNA editing. *PLoS pathogens* *11*, e1005166.

1262 Ghosh, P., Reddy, V., Swinscoe, J., Lebowitz, P., and Weissman, S. (1978).  
1263 Heterogeneity and 5'-terminal structures of the late RNAs of simian virus 40. *Journal of*  
1264 *molecular biology* *126*, 813-846.

- 1265 Good, P.J., Welch, R.C., Ryu, W.-S., and Mertz, J.E. (1988). The late spliced 19S and  
1266 16S RNAs of simian virus 40 can be synthesized from a common pool of transcripts.  
1267 *Journal of virology* 62, 563-571.
- 1268 Gottlieb, K.A., and Villarreal, L.P. (2001). Natural biology of polyomavirus middle T  
1269 antigen. *Microbiology and molecular biology reviews* 65, 288-318.
- 1270 Jiang, M., Abend, J.R., Johnson, S.F., and Imperiale, M.J. (2009a). The role of  
1271 polyomaviruses in human disease. *Virology* 384, 266-273.
- 1272 Jiang, M., Abend, J.R., Tsai, B., and Imperiale, M.J. (2009b). Early events during BK  
1273 virus entry and disassembly. *Journal of virology* 83, 1350-1358.
- 1274 Johnson, M., Zaretskaya, I., Raytselis, Y., Merezhuk, Y., McGinnis, S., and Madden,  
1275 T.L. (2008). NCBI BLAST: a better web interface. *Nucleic acids research* 36, W5-W9.
- 1276 Kamen, R., Favaloro, J., and Parker, J. (1980a). Topography of the three late mRNA's  
1277 of polyoma virus which encode the virion proteins. *Journal of virology* 33, 637-651.
- 1278 Kamen, R., Favaloro, J., Parker, J., Treisman, R., Lania, L., Fried, M., and Mellor, A.  
1279 (1980b). Comparison of polyoma virus transcription in productively infected mouse cells  
1280 and transformed rodent cell lines. Paper presented at: Cold Spring Harbor symposia on  
1281 quantitative biology (Cold Spring Harbor Laboratory Press).
- 1282 Keller, M.W., Rambo-Martin, B.L., Wilson, M.M., Ridenour, C.A., Shepard, S.S., Stark,  
1283 T.J., Neuhaus, E.B., Dugan, V.G., Wentworth, D.E., and Barnes, J.R. (2018). Direct  
1284 RNA sequencing of the coding complete influenza A virus genome. *Scientific reports* 8,  
1285 1-8.

- 1286 Kim, D., Lee, J.-Y., Yang, J.-S., Kim, J.W., Kim, V.N., and Chang, H. (2020). The  
1287 architecture of SARS-CoV-2 transcriptome. *Cell* *181*, 914-921. e910.
- 1288 Kress, M., May, E., Cassingena, R., and May, P. (1979). Simian virus 40-transformed  
1289 cells express new species of proteins precipitable by anti-simian virus 40 tumor serum.  
1290 *Journal of virology* *31*, 472-483.
- 1291 Krueger, F. (2016). Babraham Bioinformatics-Trim Galore.
- 1292 Lee, S., Micalizzi, D., Truesdell, S.S., Bukhari, S.I., Boukhali, M., Lombardi-Story, J.,  
1293 Kato, Y., Choo, M.-K., Dey-Guha, I., and Ji, F. (2020). A post-transcriptional program of  
1294 chemoresistance by AU-rich elements and TTP in quiescent leukemic cells. *Genome*  
1295 *biology* *21*, 1-23.
- 1296 Legon, S., Flavell, A.J., Cowie, A., and Kamen, R. (1979). Amplification in the leader  
1297 sequence of late polyoma virus mRNAs. *Cell* *16*, 373-388.
- 1298 Li, H. (2018). Minimap2: pairwise alignment for nucleotide sequences. *Bioinformatics*  
1299 *34*, 3094-3100.
- 1300 Loman, N.J., Quick, J., and Simpson, J.T. (2015). A complete bacterial genome  
1301 assembled de novo using only nanopore sequencing data. *Nature methods* *12*, 733-  
1302 735.
- 1303 Luo, Y., and Carmichael, G.G. (1991). Splice site skipping in polyomavirus late pre-  
1304 mRNA processing. *Journal of virology* *65*, 6637-6644.
- 1305 Nguyen, K.D., Lee, E.E., Yue, Y., Stork, J., Pock, L., North, J.P., Vandergriff, T.,  
1306 Cockerell, C., Hosler, G.A., and Pastrana, D.V. (2017). Human polyomavirus 6 and 7

1307 are associated with pruritic and dyskeratotic dermatoses. *Journal of the American*  
1308 *Academy of Dermatology* 76, 932-940. e933.

1309 Nomburg, J., Meyerson, M., and DeCaprio, J.A. (2020). Pervasive generation of non-  
1310 canonical subgenomic RNAs by SARS-CoV-2. *Genome medicine* 12, 1-14.

1311 Norbury, C.J., and Fried, M. (1987). Polyomavirus early region alternative poly (A) site:  
1312 3'-end heterogeneity and altered splicing pattern. *Journal of virology* 61, 3754-3758.

1313 Price, A.M., Hayer, K.E., McIntyre, A.B., Gokhale, N.S., Abebe, J.S., Della Fera, A.N.,  
1314 Mason, C.E., Horner, S.M., Wilson, A.C., and Depledge, D.P. (2020). Direct RNA  
1315 sequencing reveals m 6 A modifications on adenovirus RNA are necessary for efficient  
1316 splicing. *Nature communications* 11, 1-17.

1317 Quinlan, A.R., and Hall, I.M. (2010). BEDTools: a flexible suite of utilities for comparing  
1318 genomic features. *Bioinformatics* 26, 841-842.

1319 Reddy, V.B., Ghosh, P.K., Lebowitz, P., and Sherman M, W. (1978). Gaps and  
1320 duplicated sequences in the leaders of SV40 16S RNA. *Nucleic acids research* 5, 4195-  
1321 4214.

1322 Riley, M.I., Yoo, W., Mda, N.Y., and Folk, W.R. (1997). Tiny T antigen: an autonomous  
1323 polyomavirus T antigen amino-terminal domain. *Journal of virology* 71, 6068-6074.

1324 Rosenstein, R.K., Pastrana, D.V., Starrett, G.J., Sapio, M.R., Hill, N.T., Jo, J.-H., Lee,  
1325 C.-C.R., Iadarola, M.J., Buck, C.B., and Kong, H.H. (2021). Host-Pathogen Interactions  
1326 in Human Polyomavirus 7–Associated Pruritic Skin Eruption. *The Journal of*  
1327 *investigative dermatology* 141, 1344-1348. e1348.

- 1328 Saribas, A.S., DeVoto, J., Golla, A., Wollebo, H.S., White, M.K., and Safak, M. (2018).  
1329 Discovery and characterization of novel trans-spliced products of human polyoma JC  
1330 virus late transcripts from PML patients. *Journal of cellular physiology* *233*, 4137-4155.
- 1331 Schmidlin, K., Kraberger, S., Cook, C., DeNardo, D.F., Fontenele, R.S., Van Doorslaer,  
1332 K., Martin, D.P., Buck, C.B., and Varsani, A. (2021). A novel lineage of polyomaviruses  
1333 identified in bark scorpions. *bioRxiv*.
- 1334 Seif, I., Khoury, G., and Dhar, R. (1979). The genome of human papovavirus BKV. *Cell*  
1335 *18*, 963-977.
- 1336 Shuda, M., Feng, H., Kwun, H.J., Rosen, S.T., Gjoerup, O., Moore, P.S., and Chang, Y.  
1337 (2008). T antigen mutations are a human tumor-specific signature for Merkel cell  
1338 polyomavirus. *Proceedings of the National Academy of Sciences* *105*, 16272-16277.
- 1339 Smith, A.E., Smith, R., and Paucha, E. (1979). Characterization of different tumor  
1340 antigens present in cells transformed by simian virus 40. *Cell* *18*, 335-346.
- 1341 Starrett, G.J., Thakuria, M., Chen, T., Marcelus, C., Cheng, J., Nomburg, J., Thorner,  
1342 A.R., Slevin, M.K., Powers, W., and Burns, R.T. (2020). Clinical and molecular  
1343 characterization of virus-positive and virus-negative Merkel cell carcinoma. *Genome*  
1344 *medicine* *12*, 1-22.
- 1345 Starrett, G.J., Yu, K., Golubeva, Y., Lenz, P., Piaskowski, M.L., Peterson, D., Dean, M.,  
1346 Israni, A., Hernandez, B.Y., Tucker, T.C., *et al.* (2021). Common Mechanisms of Virus-  
1347 Mediated Oncogenesis in Bladder Cancers Arising In Solid Organ Transplant  
1348 Recipients. *medRxiv*, 2021.2011.2011.21266080.

- 1349 Theiss, J.M., Günther, T., Alawi, M., Neumann, F., Tessmer, U., Fischer, N., and  
1350 Grundhoff, A. (2015). A comprehensive analysis of replicating Merkel cell polyomavirus  
1351 genomes delineates the viral transcription program and suggests a role for mcv-miR-M1  
1352 in episomal persistence. *PLoS pathogens* *11*, e1004974.
- 1353 Treisman, R. (1980). Characterisation of polyoma late mRNA leader sequences by  
1354 molecular cloning and DNA sequence analysis. *Nucleic acids research* *8*, 4867-4888.
- 1355 Tremblay, J.D., Sachsenmeier, K.F., and Pipas, J.M. (2001). Propagation of wild-type  
1356 and mutant SV40. In *SV40 Protocols* (Springer), pp. 1-7.
- 1357 Trowbridge, P.W., and Frisque, R.J. (1995). Identification of three new JC virus proteins  
1358 generated by alternative splicing of the early viral mRNA. *Journal of neurovirology* *1*,  
1359 195-206.
- 1360 Yang, R., Lee, E.E., Kim, J., Choi, J.H., Kowitz, E., Chen, Y., Crewe, C., Salisbury, N.J.,  
1361 Scherer, P.E., and Cockerell, C. (2021). Characterization of ALTO-encoding circular  
1362 RNAs expressed by Merkel cell polyomavirus and trichodysplasia spinulosa  
1363 polyomavirus. *PLoS pathogens* *17*, e1009582.
- 1364 Zerrahn, J., Knippschild, U., Winkler, T., and Deppert, W. (1993). Independent  
1365 expression of the transforming amino-terminal domain of SV40 large T antigen from an  
1366 alternatively spliced third SV40 early mRNA. *The EMBO journal* *12*, 4739-4746.
- 1367 Zhao, L., and Imperiale, M.J. (2019). Establishing Renal Proximal Tubule Epithelial-  
1368 Derived Cell Lines Expressing Human Telomerase Reverse Transcriptase for Studying  
1369 BK Polyomavirus. *Microbiology resource announcements* *8*, e01129-01119.

1370 Zou, W., Vue, G.S., Assetta, B., Manza, H., Atwood, W.J., and Imperiale, M.J. (2020).

1371 Control of archetype BK polyomavirus microRNA expression. *Journal of Virology* 95,

1372 e01589-01520.

1373

1374

## Figure 1

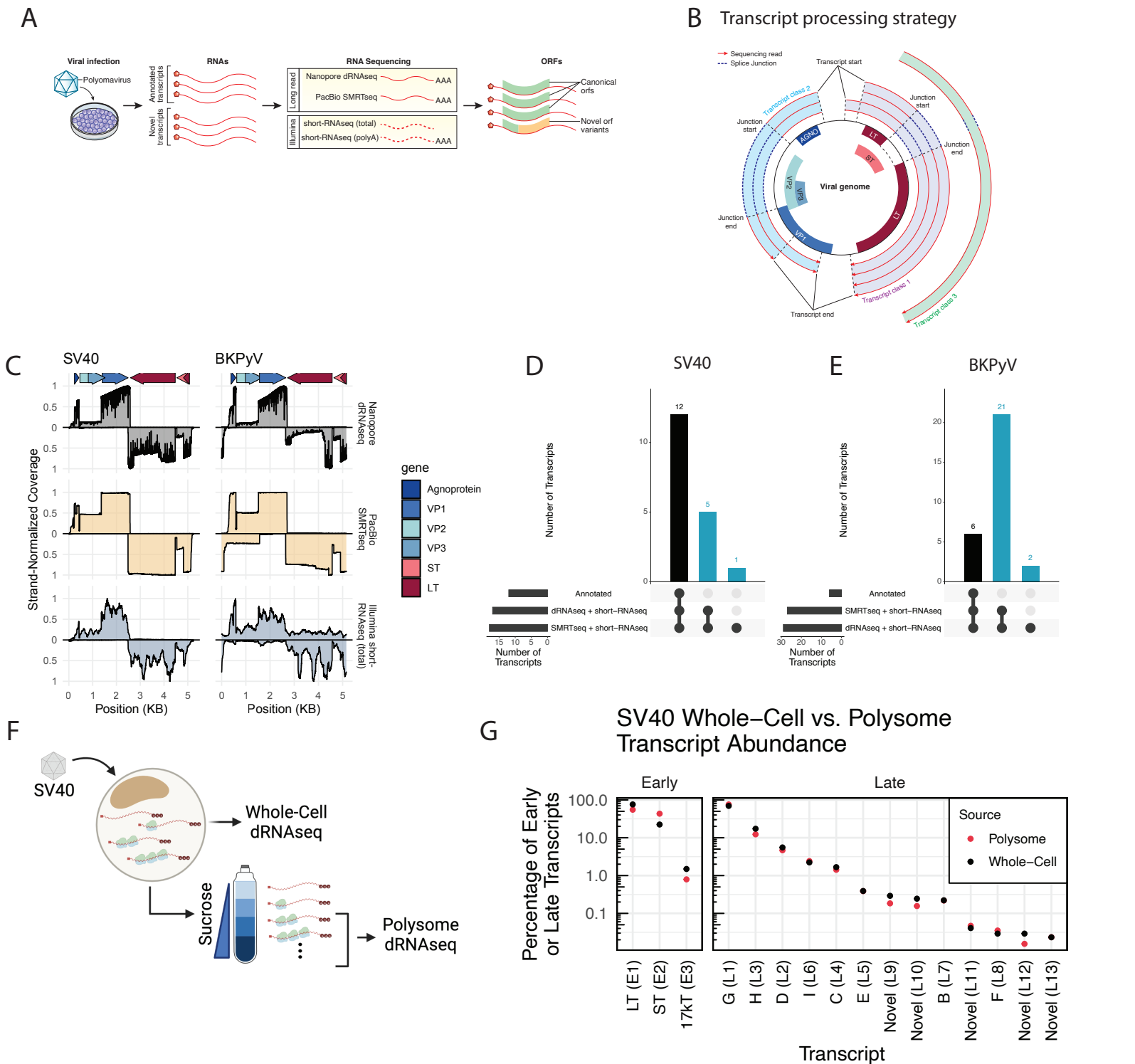


Figure 1 - RNA sequencing expands known SV40 and BKPyV transcript diversity.

A. Overview of experimental procedures. Cells were infected with a polyomavirus, and RNAs extracted. RNA was sequenced using long-read (Nanopore dRNAseq and PacBio SMRTseq) and short-read (Illumina short-RNAseq (total) and short-RNAseq (polyA)). Transcripts were analyzed, and the impact of observed splice events on viral open reading frames was assessed.

B. Mechanism of transcript clustering in this study. Transcripts were aligned to the viral genome and grouped into transcript classes based on the presence of shared introns. Thus, within a transcript class there may be variation in the exact transcript start and end positions. This clustering strategy was used for both long- and short-RNAseq data.

C. Viral RNA sequence coverage for SV40 and BKPyV as determined from dRNAseq, SMRTseq, and short-RNAseq (total) data. The Y axis indicates the scaled coverage, with X axis indicating the position on the viral genome. Coverage for late transcripts (mapping to the + strand) is above the x axis, while coverage for early transcripts (mapping to the - strand) is below the x axis. Coverage is scaled separately for each strand such that the maximum observed coverage for each strand is 1. Arrows at the top of the plot indicate the positions of viral genes.

D-E. UpSet plot indicating the overlap between existing transcript annotations, dRNAseq data, and SMRTseq data for SV40 (D) and BKPyV Dunlop (E). Bars indicating overlap with existing transcript annotations are black, while those indicating no overlap with existing annotations are blue. These blue bars indicate the number of novel, unannotated transcripts identified.

F. Overview of polysome profiling of SV40-infected cells. BSC40 cells were infected with SV40. Cells were lysed, and a portion of the lysate was subjected to dRNAseq (representative of the RNA content of the whole cell). The remaining lysates was centrifuged through a sucrose gradient, after which fractions containing RNA associated with two or more ribosomes were pooled and subjected to dRNAseq.

G. Relative abundance of SV40 early and late transcripts in the whole-cell and polysome fractions of SV40-infected cells. Y-axis indicates the percentage of early or late transcripts and is log scale. X axis indicates each transcript, with black dots indicating each transcript's whole-cell relative abundance and red dots indicating each transcript's polysome relative abundance.





## Figure 3

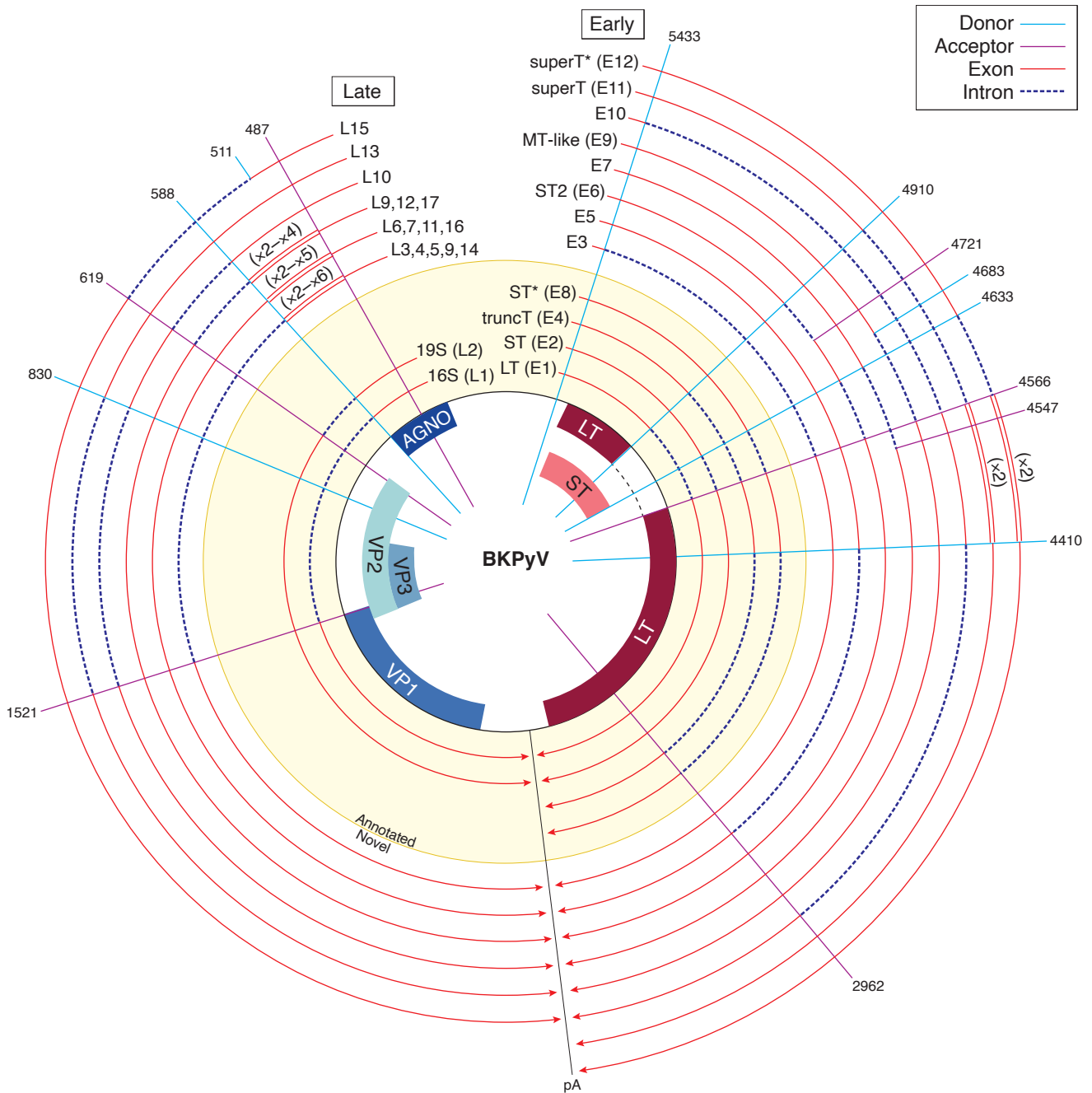
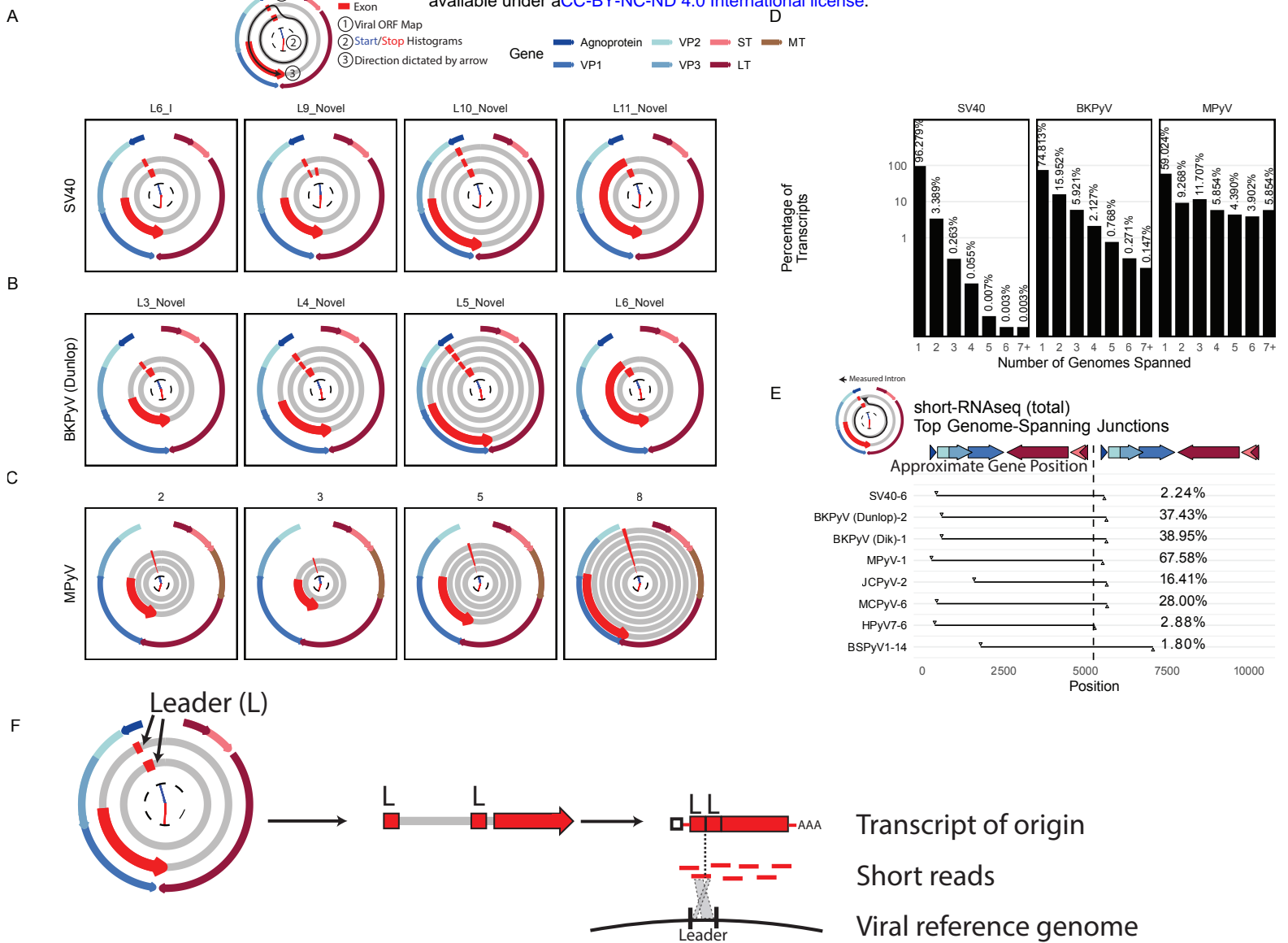


Figure 3 - Annotated and novel BKPyV transcripts.

A. Transcripts are shown relative to the viral genome. Each line is a viral transcript, with red lines indicating exons and dashed blue lines indicating introns. Spikes indicate the positions of common splice donors and splice acceptors. Transcripts that were annotated prior to this study are on a yellow background, and novel transcripts are on a white background. Wraparound transcription that results in multiple copies of a region is annotated with double lines, and the number of copies is indicated in parentheses. The line labeled "pA" indicates the approximate position of the polyA signal sequence.

Figure 4



**Figure 4 - Pervasive wraparound transcription across PyV**

A-C. Watch plots indicating the top 4 highest abundance late wraparound transcript classes in dRNAseq data from SV40 (A), BKPyV Dunlop (B), and MPyV (C). The outer ring of each watch plot indicates the position of the viral ORFs. The inner arms are histograms detailing the distribution of transcript starts (in blue) and ends (in red) for transcripts within each transcript class. The red segments indicate exons. Transcripts start in the innermost ring - a second or third ring indicates that the pre-mRNA that generated the transcript must have circled the viral genome multiple times. The 3' end of the transcript and the direction in which these plots are oriented is indicated by the red arrow at the end of the last exon segment. The red exon segments start at the most common transcript start site within the transcript class, and end at the most common transcript end site within the class. The watch plot key shows an example of the path of the pre-mRNA for SV40 transcript class L6\_I.

D. Bar plots indicating the percentage of late transcripts that span a given number of genome lengths in SV40, BKPyV Dunlop, and MPyV dRNAseq data.

E. The leader-leader junction, that connects the pre-mRNA from one genome to the subsequent wraparound, was identified in Illumina short-RNAseq (total) data. The intron in question is plotted as a black line in this plot, with the x axis indicating the genomic position of the intron. The top late wraparound transcript for each virus was plotted.

The gene map indicates the approximate gene position and is accurate for SV40 - the exact position of the viral genes varies between viruses. Percentages indicate the percentage of late junction-spanning transcripts that support the plotted wraparound leader-leader junction.

F. Schematic illustrating how leader-leader wraparound transcription can be detected from short read short-RNAseq (total). Leader-leader splicing can be seen as a repetitive exon in watch plots from long-read RNAseq data. Ultimately, there was an original processed mRNA in the cell that contained two tandem leader sequences. When this transcript of origin is sequenced via short read sequencing, reads will be generated across its length. A minority of these reads will span the leader-leader junction, and mapping against the viral reference genome can be used to uncover leader-leader splicing.



**Figure 5 - Detection of novel, conserved splicing events that expand PyV coding capacity.**

A-D. Schematics illustrating identified ORFs. Each row is a reading frame (except for ST and the LT 1st exon, which are in the same frame), and unannotated amino acids are represented by grey boxes. The measured intron is indicated by the red arrow. Colored ORFs are annotated, while grey ORFs are unannotated. Percentages on the right side of the figure are the percentage of spliced viral transcripts on the same strand as determined from short-read short-RNAseq (total) data. Numbers after each virus name indicate the transcript class within each short-RNAseq (total) dataset. The measured intron is indicated by the red arrow.

A) ST2: This ORF is generating from a splicing event that uses the LT first exon donor and an acceptor within the ST ORF. In HPyV7 and BKPyV Dunlop, the splice lands in frame and results in an internal deletion within ST. In MPyV and MCPyV the splice lands out of frame, resulting in an ORF that contains the N-terminal region of ST and novel amino acids at the C terminus.

B) MT: MPyV encodes a MT following splicing connecting the end of the ST ORF with an ORF in an alternate frame of the LT second exon. In BKPyV, a similar splice occurs connecting ST with an MT-like ORF in an alternative frame of the LT second exon.

C) VP1X: JCPyV encodes two VP1X ORFs generated by splicing within VP1 and landing in an alternative frame of VP1, or earlier in the late region due to wraparound transcription. While predominant in JCPyV, VP1X is likewise present in many other PyV.

D) superT: The superT-specific splice utilizes the splice donor canonically associated with truncated T antigens such as 17kT in SV40 and truncT in BKPyV. Due to wraparound transcription, a LT second exon acceptor is available to the 3' of this donor and acts as the acceptor. For the superT ORF to form, an initial LT splice is required. Ultimately, superT contains a duplication in part of the LT second exon that includes the RB-binding LxCxE motif.

E. Schematics detailing BKPyV Dik isolates used for querying the existence of superT. BKPyV WT is wild type virus. M1 contains a LT intron that has been replaced with an intron from the plasmid pCI. Both WT and M1 are expected to generate LT and superT of expected sizes. M2 has a completely removed LT intron, and the pCI intron is located directly 5' of the LT ORF. M2 is expected to encode LT of expected size, but a larger superT variant due to incorporation of a second copy of the LT first exon.

F. Western blot of cells infected with BKPyV Dik WT, M1, or M2 and probed with an antibody reactive against LT. The lower molecular weight band is LT, and the higher molecular weight bands are consistent with superT.

## Figure 6

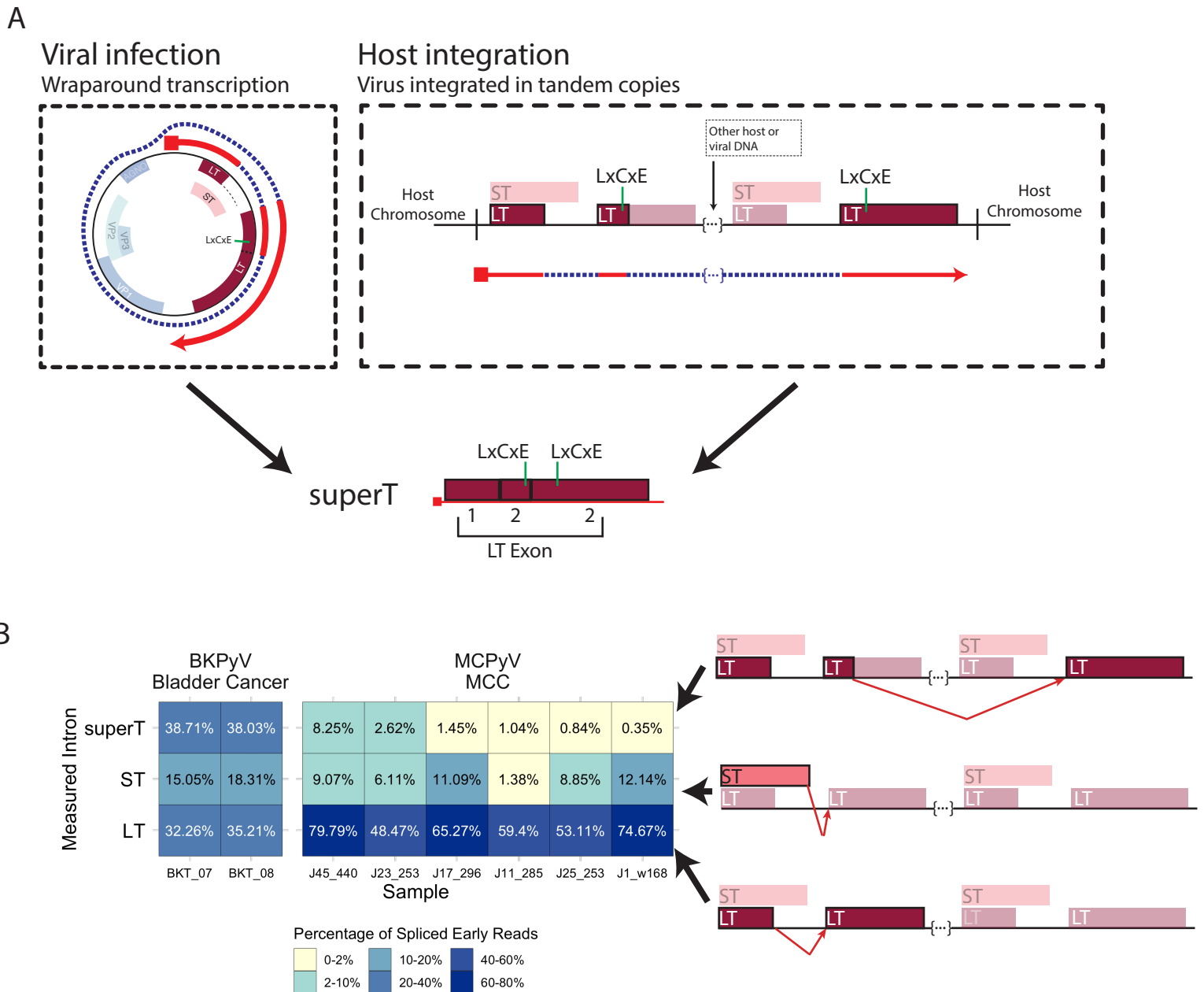


**Figure 6 - Detection superT-encoding transcripts in PyV-associated cancers**

A. Schematic detailing the generation of superT during lytic infection as compared to from integrated virus in cancer. During viral infection, the RNA polymerase can circle the viral genome multiple times, resulting in a pre-mRNA that can be spliced to generate superT. In the case of host integration, a polyomavirus can be integrated in tandem copies such that a pre-mRNA is generated with more than one copy of the viral early region. This pre-mRNA can be similarly spliced to generate a superT transcript.

B. Heatmap indicating the abundance of the superT, ST, and LT introns from RNAseq data from two replicates of a BKPyV-positive bladder cancer and six MCPyV-associated MCCs. Percentages indicate the percentage of spliced early viral reads for each sample. The splice measured in each row is indicated by the red arrow in the schematics on the right side of the figure.

Fig S1

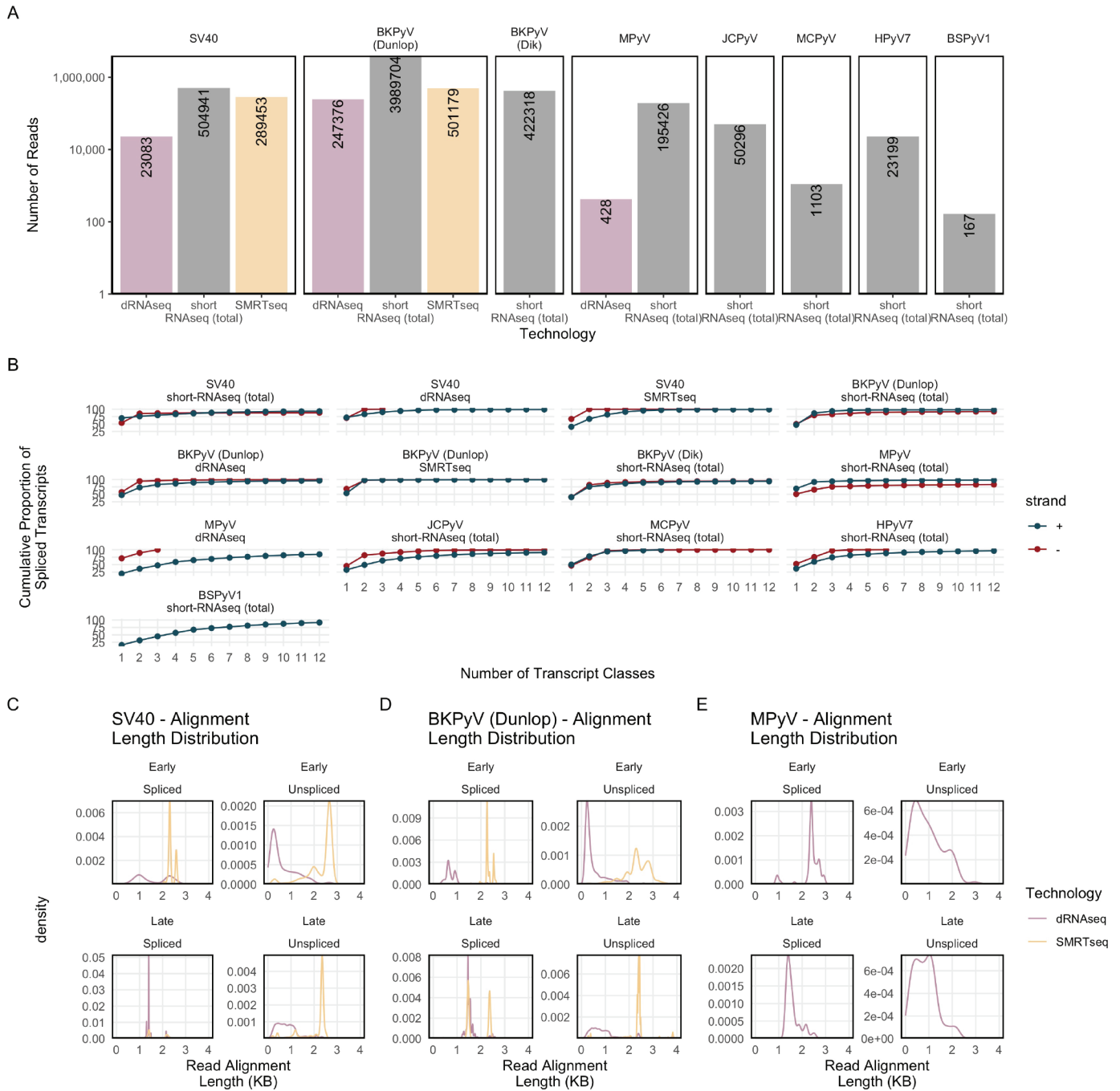
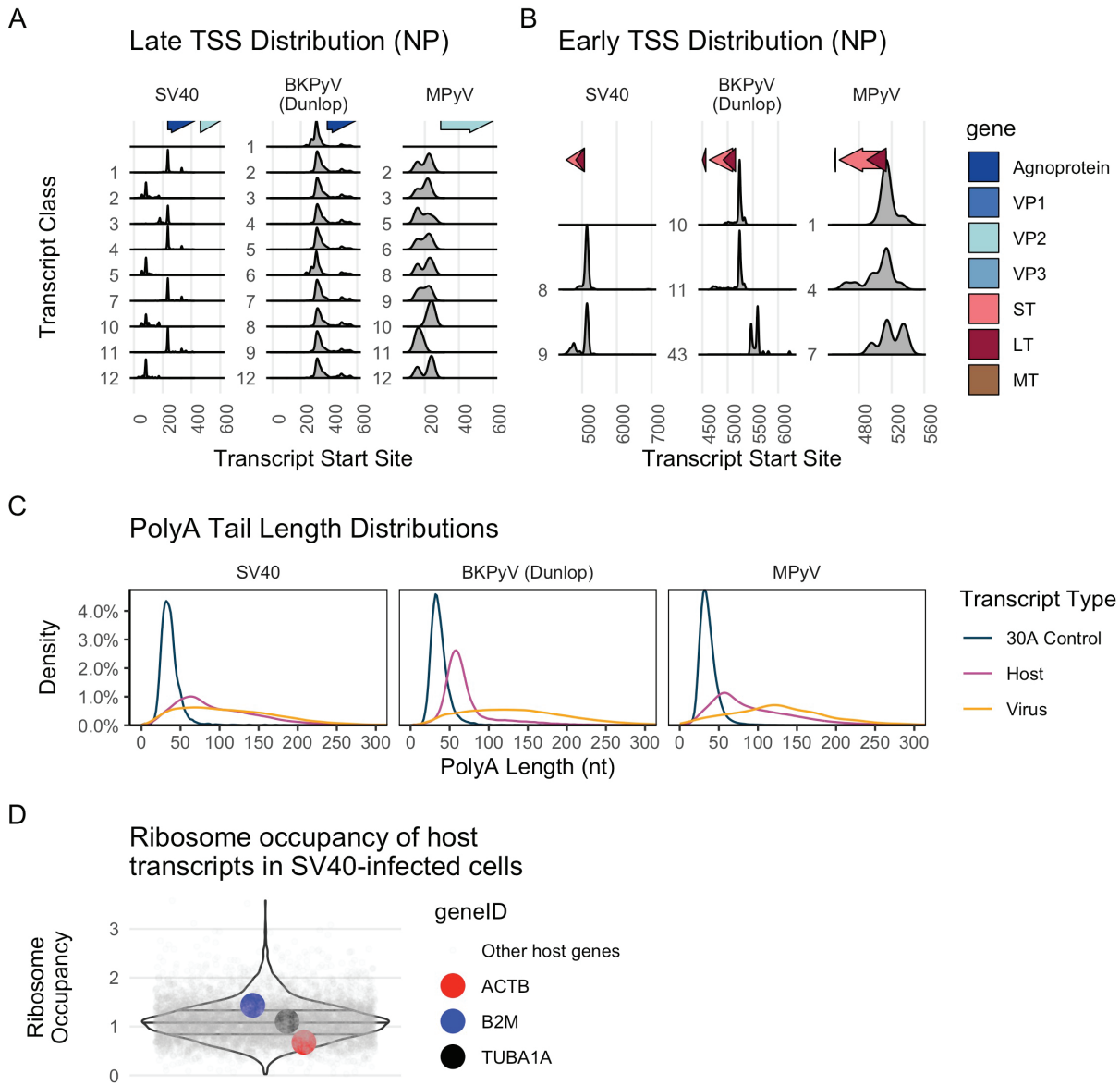


Figure S2

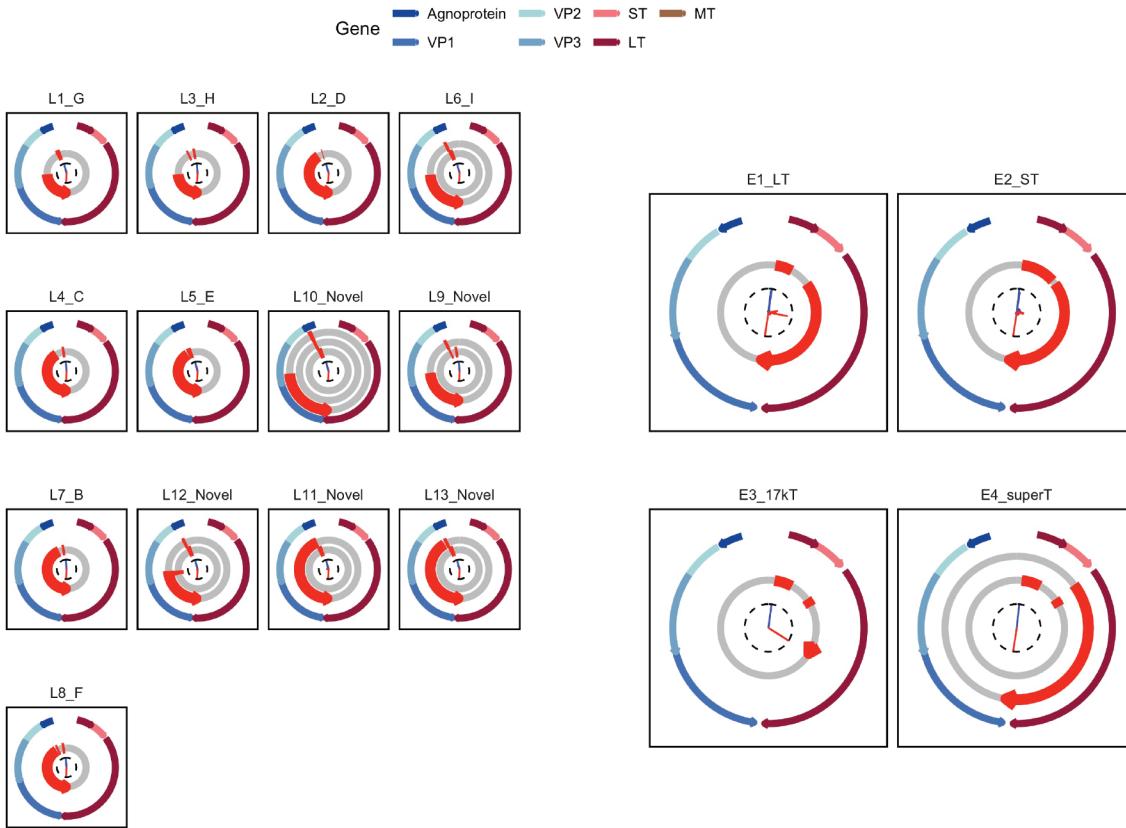




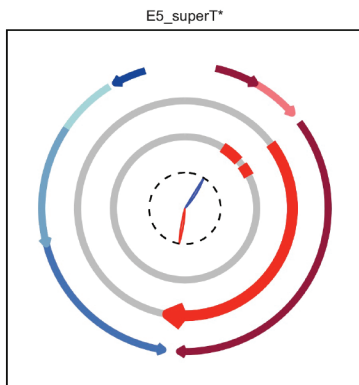
FigS3: SV40 Transcriptome

A SV40: dRNAseq + SMRTseq, Late

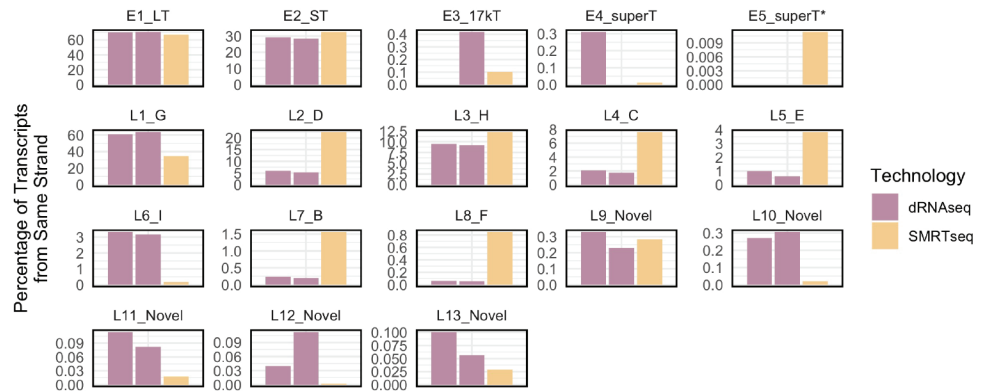
B SV40: dRNAseq + SMRTseq, Early



C SV40: SMRTseq Only



D

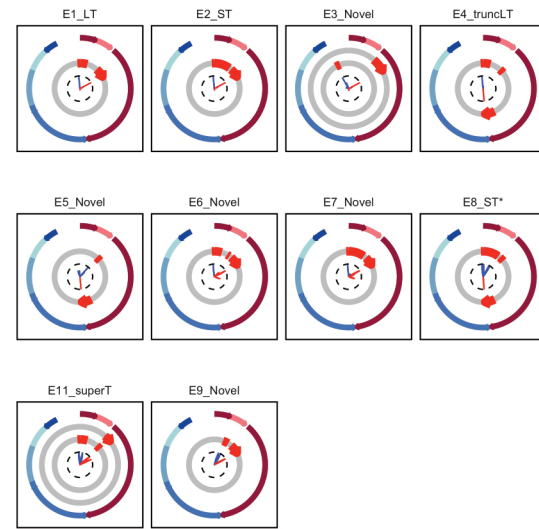
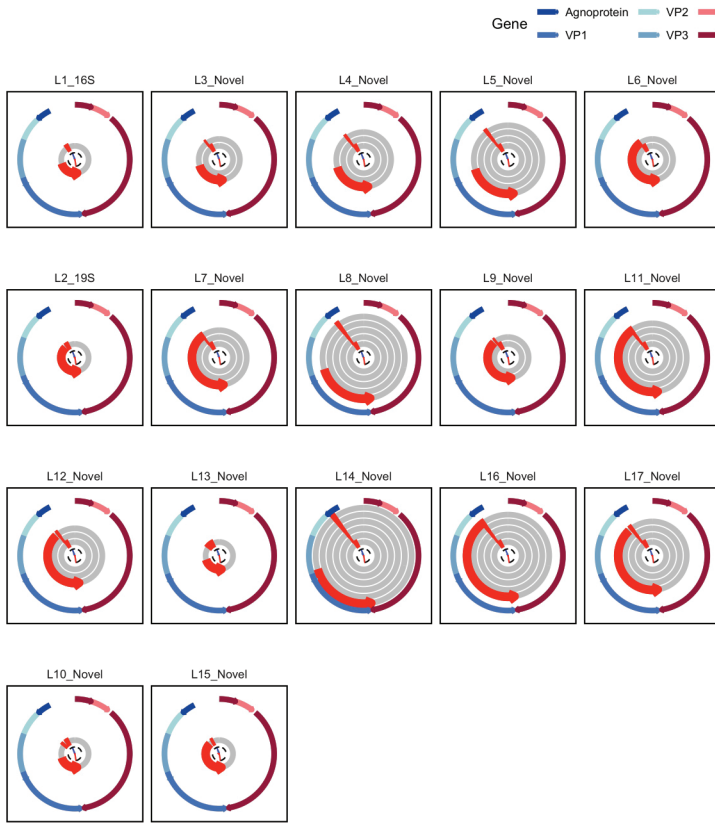




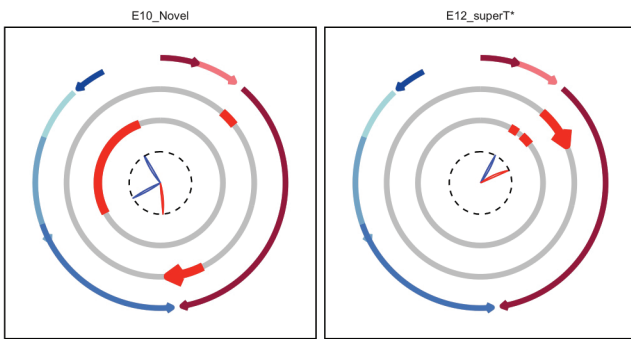
FigS4: BKPyV (Dunlop) Transcriptome

A BKPyV (Dunlop): dRNAseq + SMRTseq, Late

B BKPyV (Dunlop): dRNAseq + SMRTseq, Early



C BKPyV (Dunlop): dRNAseq Only



D

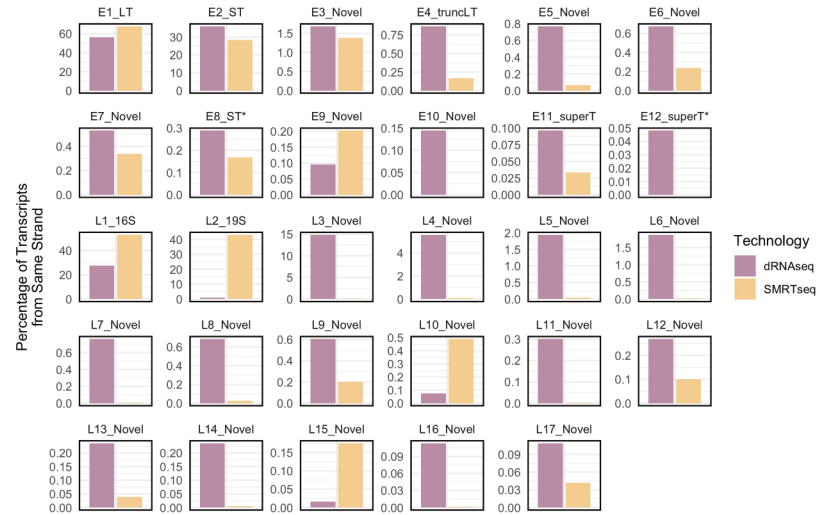


Fig S5: SV40 Late Transcript Pileups

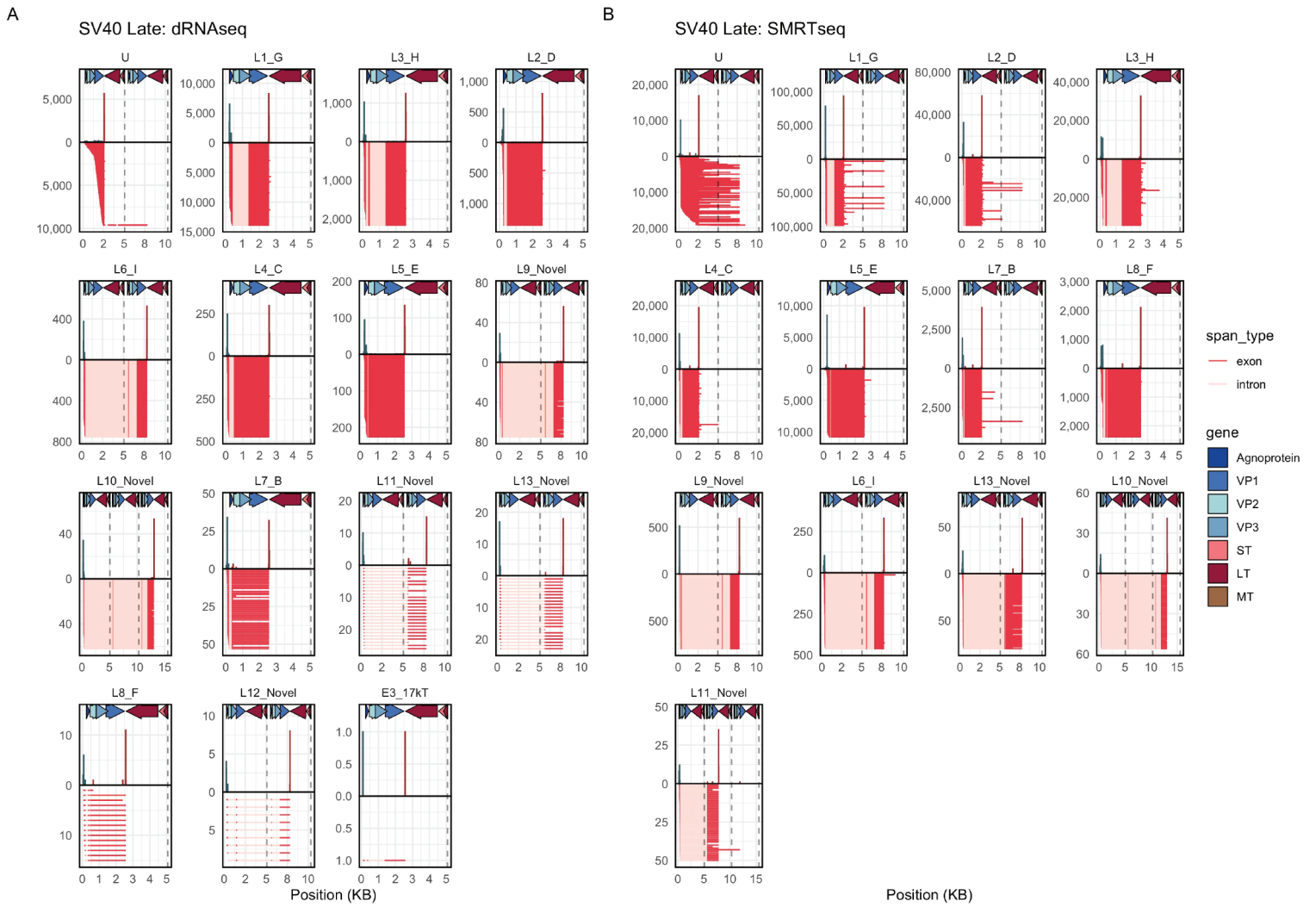


Fig S6: SV40 Early Transcript Pileups

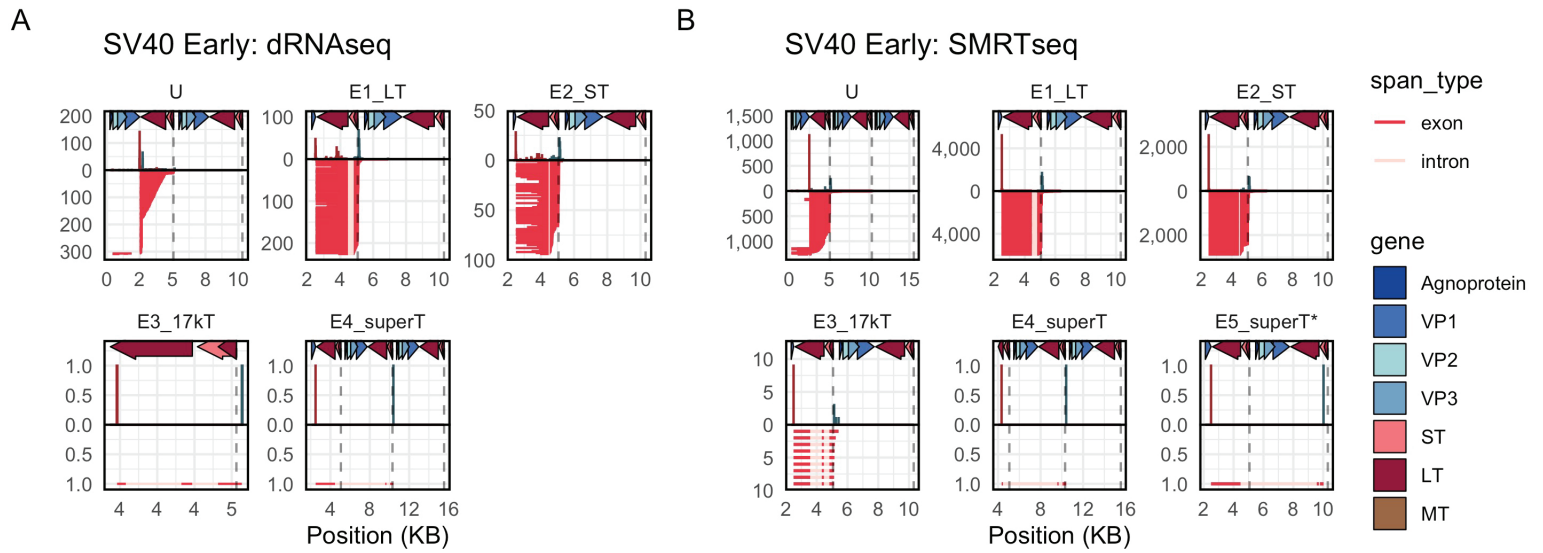


Fig S7: BKPyV (Dunlop) Late Transcript Pileups

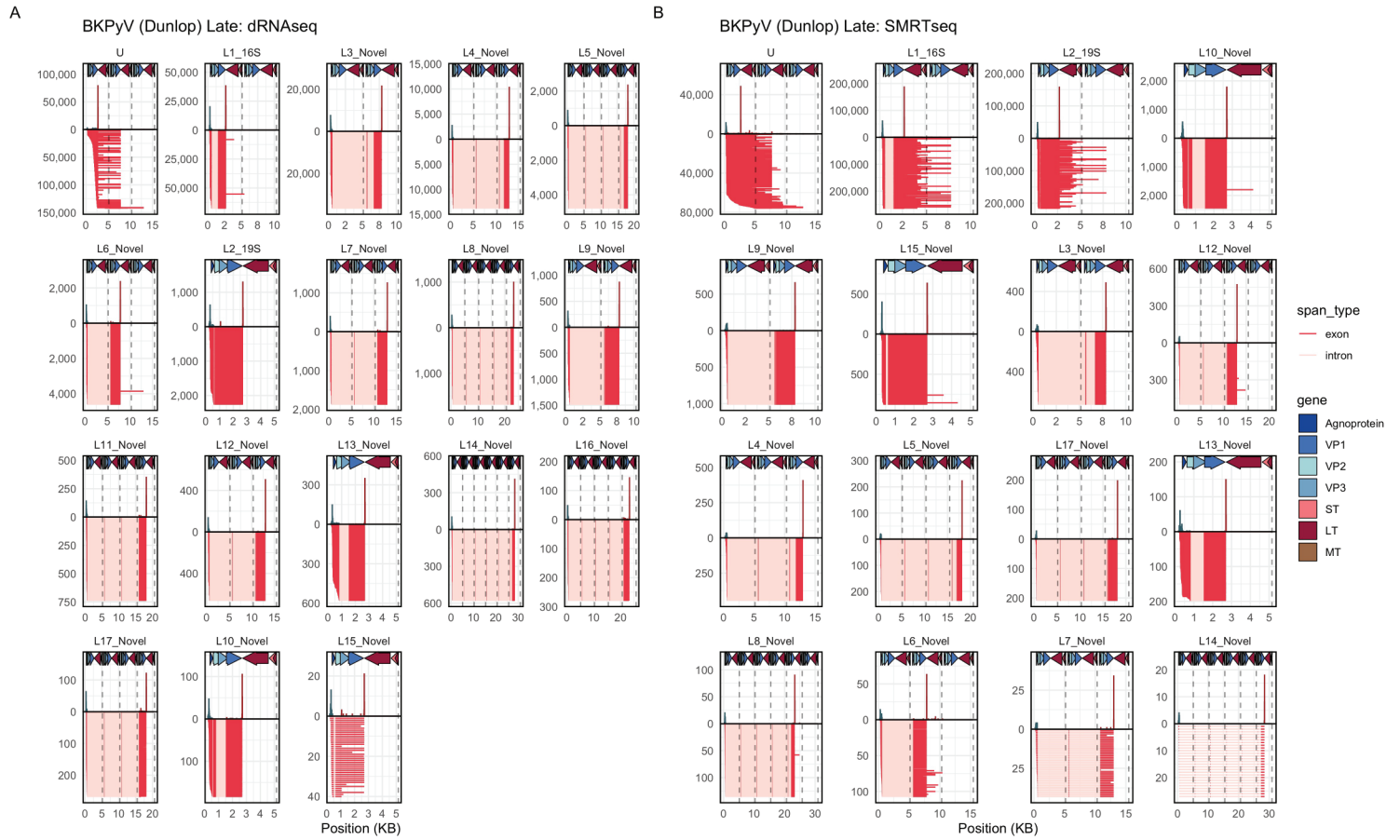
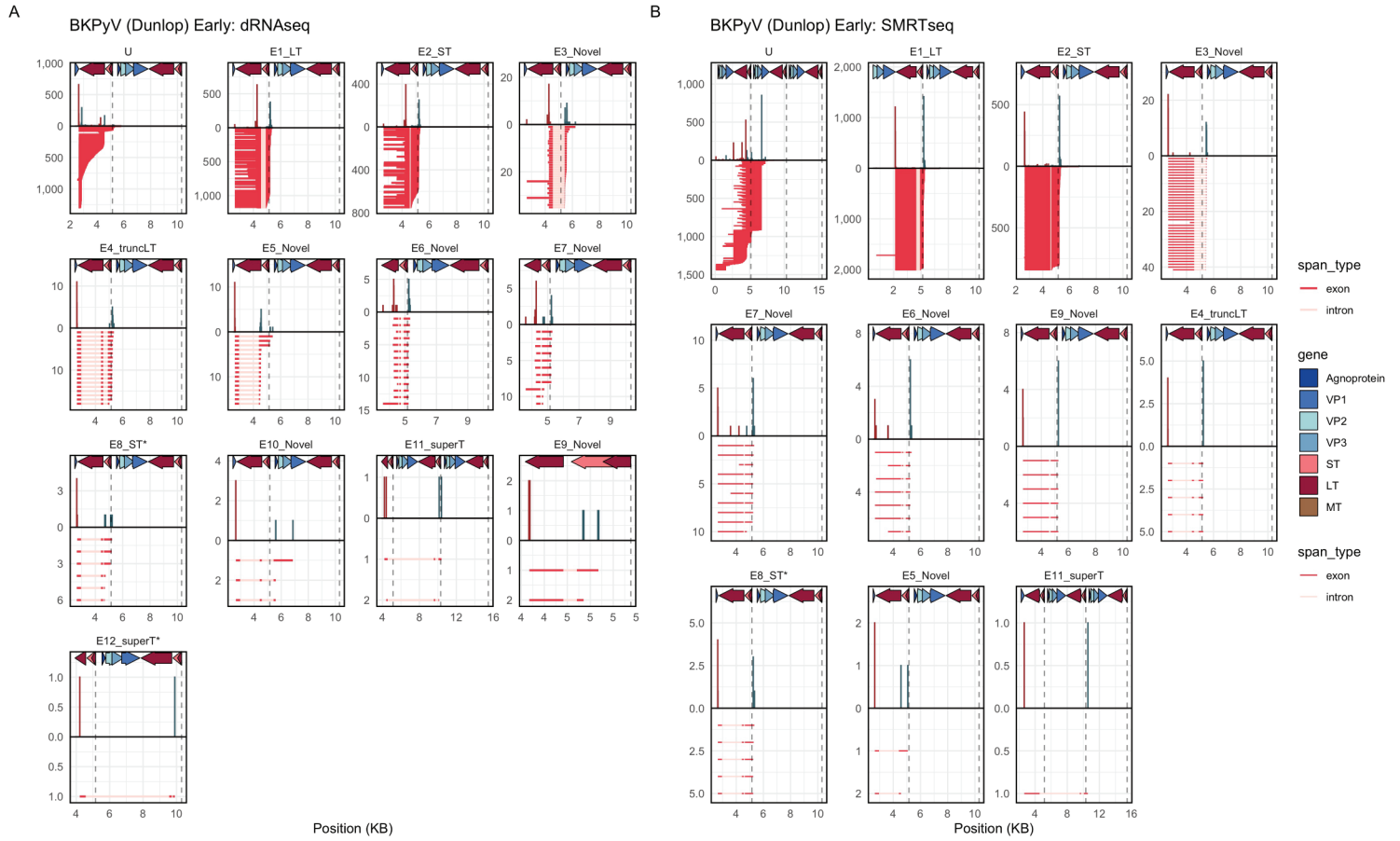
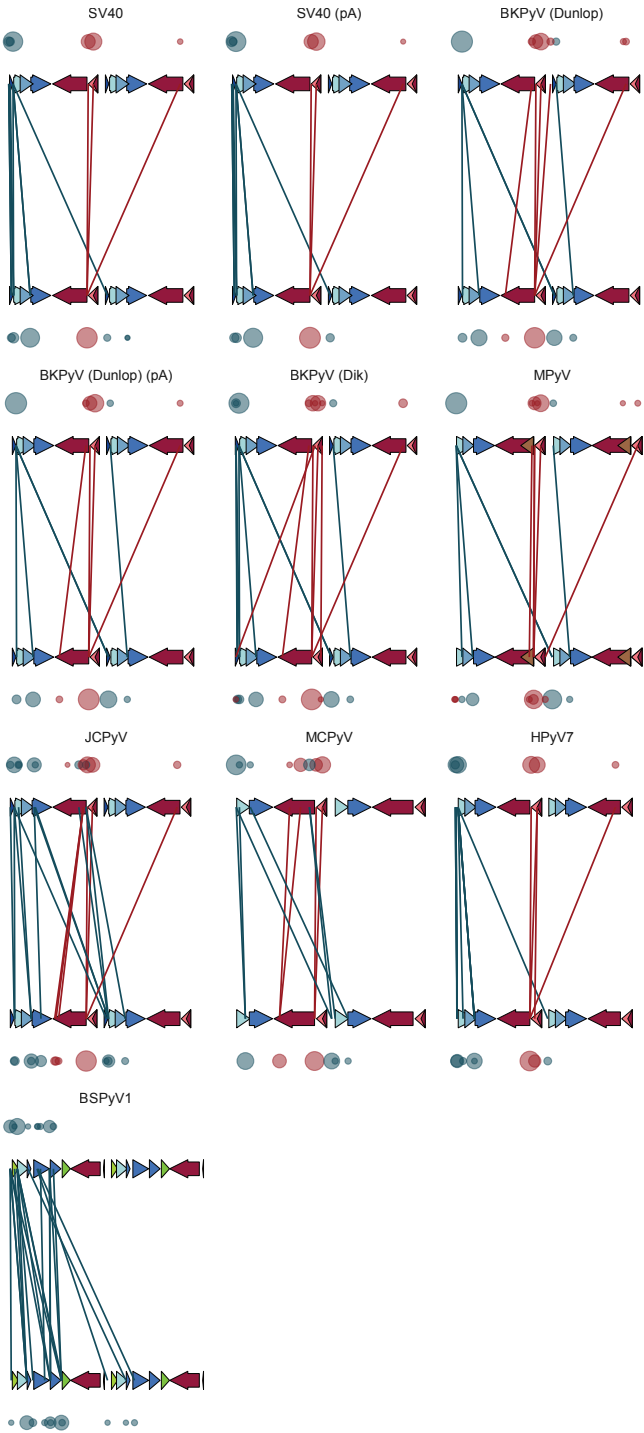


Fig S8: BKPyV (Dunlop) Early Transcript Pileups



A



B

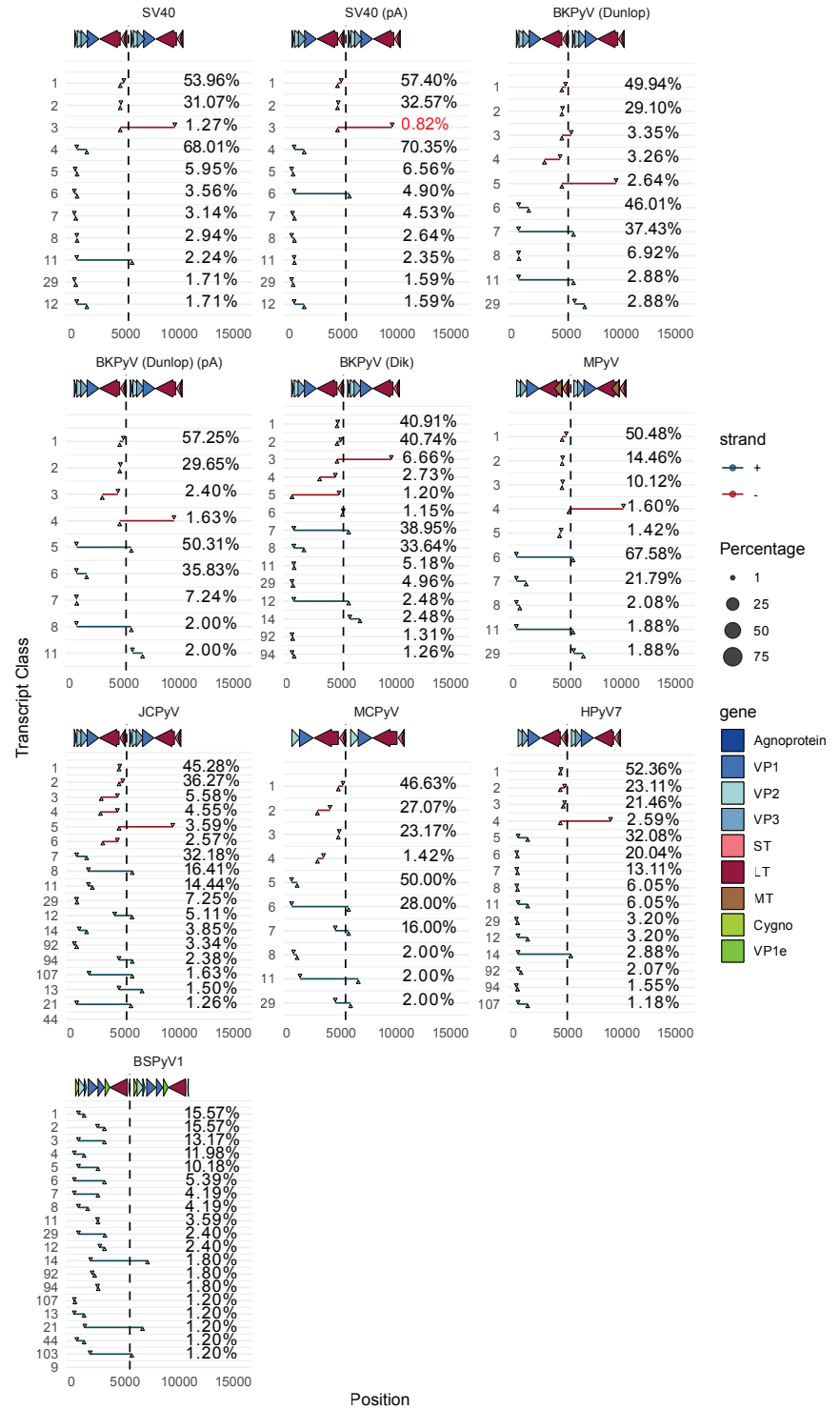


Figure S10

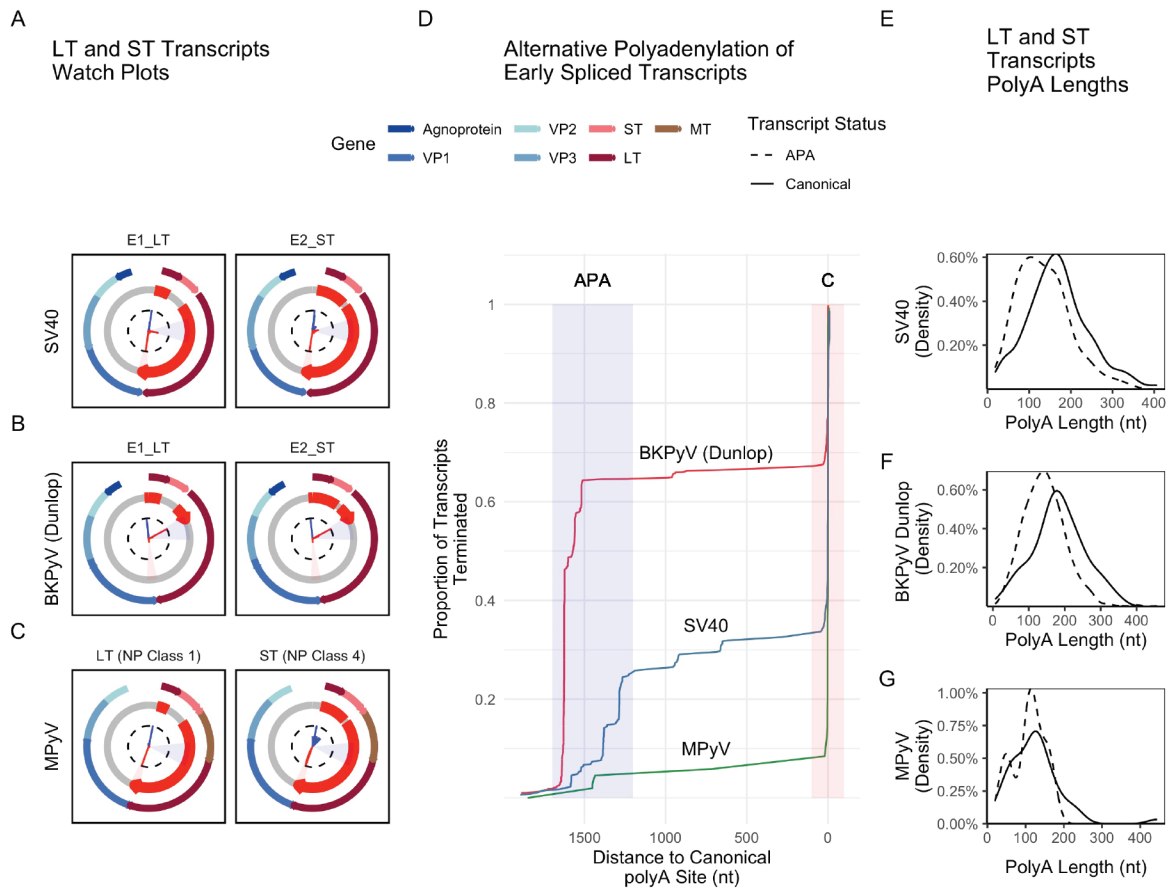
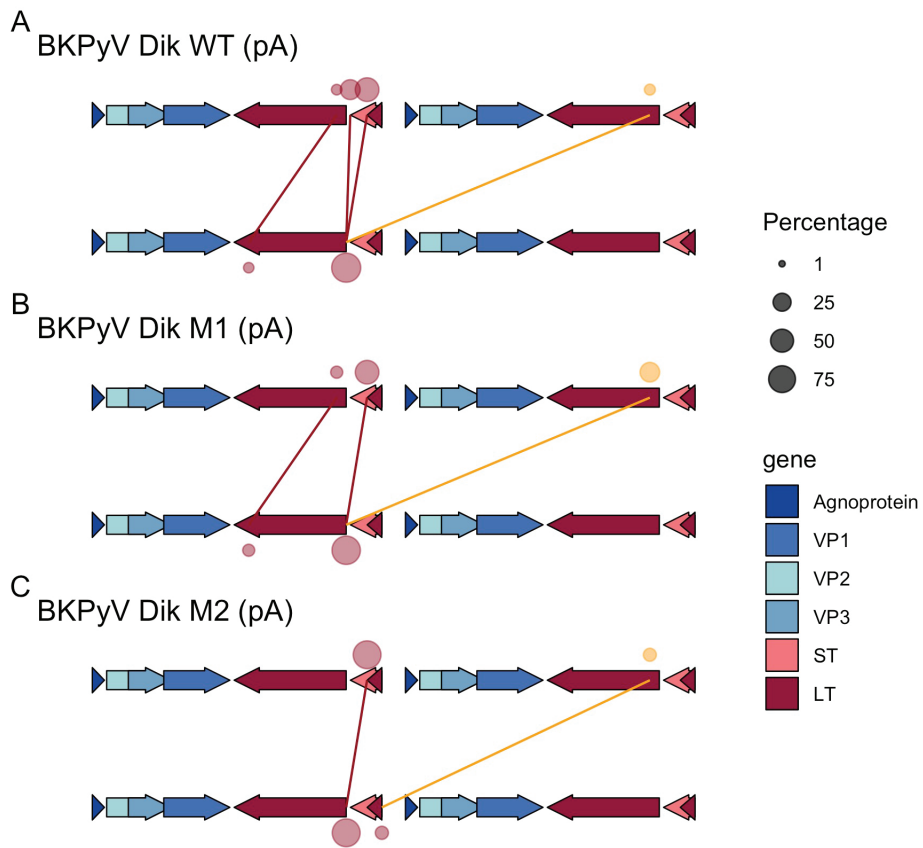




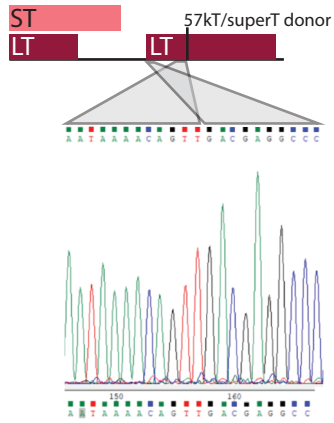
Fig S11

BKPyV Dik short-RNaseq (polyA)

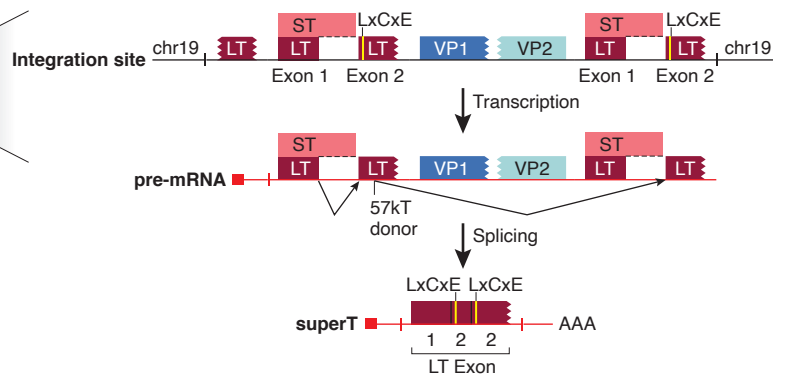
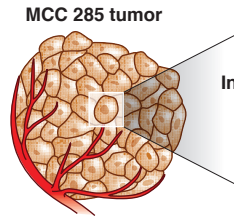




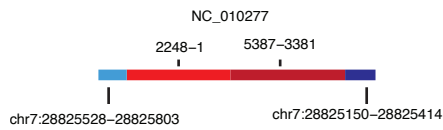
A Tumor: J45\_440



B



C Tumor: J45\_440



D Tumor: J17\_296



E

